The IplA Ca^{2+} channel of *Dictyostelium discoideum* is necessary for chemotaxis mediated through Ca^{2+}, but not through cAMP, and has a fundamental role in natural aggregation

Daniel F. Lusche, Deborah Wessels, Amanda Scherer, Karla Daniels, Spencer Kuhl and David R. Soll*

W. M. Keck Dynamic Image Analysis Facility, Department of Biology, University of Iowa, Iowa City, IA 52242, USA

*Author for correspondence (david-soll@uiowa.edu)

Accepted 5 December 2011
Journal of Cell Science 125, 1770–1783

doi: 10.1242/jcs.098301

Summary

During aggregation of *Dictyostelium discoideum*, nondissipating, symmetrical, outwardly moving waves of cAMP direct cells towards aggregation centers. It has been assumed that the spatial and temporal characteristics of the front and back of each cAMP wave regulate both chemokinesis and chemotaxis. However, during the period preceding aggregation, cells acquire not only the capacity to chemotax in a spatial gradient of cAMP, but also in a spatial gradient of Ca^{2+}. The null mutant of the putative IplA Ca^{2+} channel gene, *iplA*$^{-}$, undergoes normal chemotaxis in spatial gradients of cAMP and normal chemokinetic responses to increasing temporal gradients of cAMP, both generated in vitro. However, *iplA*$^{-}$ cells lose the capacity to undergo chemotaxis in response to a spatial gradient of Ca^{2+}, suggesting that IplA is either the Ca^{2+} chemotaxis receptor or an essential component of the Ca^{2+} chemotaxis regulatory pathway. In response to natural chemotactic waves generated by wild-type cells, the chemokinetic response of *iplA*$^{-}$ cells to the temporal dynamics of the cAMP wave is intact, but the capacity to reorient in the direction of the aggregation center at the onset of each wave is lost. These results suggest that transient Ca^{2+} gradients formed between cells at the onset of each natural cAMP wave augment reorientation towards the aggregation center. If this hypothesis proves correct, it will provide a more complex contextual framework for interpreting *D. discoideum* chemotaxis.

Key words: cAMP chemotaxis, Microfluidic chamber, Ca^{2+} binding, Inositol trisphosphate receptor, Mechanoreceptor

Introduction

Extracellular cations play essential roles in cell polarity, motility and chemotaxis (Soll et al., 2011). For that reason, they must be present at optimum concentrations in the natural environment (Soll et al., 2011). For the soil amoeba *Dictyostelium discoideum* to achieve maximum velocity either the extracellular concentration of Ca^{2+} must reach 10 mM or the concentration of K^{+} reach 40 mM (Lusche et al., 2009; Lusche et al., 2011; Scherer et al., 2010). Moreover, for *D. discoideum* amoebae to orient in a spatial gradient of the chemoattractant cAMP, either Ca^{2+} must reach 5 mM, or K^{+} or Na^{+} reach 15 mM (Lusche et al., 2009; Lusche et al., 2011). In addition to its role in facilitating motility and chemotactic orientation, Ca^{2+} also acts as a chemoattractant. When developing cells attain chemotactic responsiveness to spatial gradients of extracellular cAMP, they also attain chemotactic responsiveness to spatial gradients of extracellular Ca^{2+} (Scherer et al., 2010). Deletion of the gene for the putative sodium/hydrogen exchanger Nhe1 (NheA) (Patel and Barber, 2005) resulted in the loss of K^{+} as a facilitator of polarity and motility, and the loss of Na^{+} or K^{+} as a facilitator of chemotactic orientation in a spatial gradient of cAMP (Lusche et al., 2011). Deletion of Nhe1, however, did not affect Ca^{2+} facilitation of these behaviors (Lusche et al., 2011). These results indicated that one or more plasma membrane proteins other than Nhe1 was involved in the facilitation of motility and chemotaxis by Ca^{2+} (Lusche et al., 2011).

To identify these membrane proteins, we first searched for, but did not find in *D. discoideum*, an ortholog of CaR, a bona fide G-protein-coupled Ca^{2+} receptor (Brown et al., 1993; Garrett et al., 1995; Brown and MacLeod, 2001; Khan and Conigrave, 2010) involved in motility and chemotaxis in higher animal cells (Boudot et al., 2010). We therefore turned our attention to inositol 1,4,5-triphosphate receptor-like protein A (IplA), a membrane protein in *D. discoideum* with homology to the inositol trisphosphate receptors (InsP_3Rs) of higher eukaryotes (Traynor et al., 2000). These six transmembrane proteins function as homotetrameric Ca^{2+} channels (Taylor and Laude, 2002; Foskett et al., 2007; Foskett, 2010), possessing a long cytoplasmic N-terminal region with a binding site for InsP_3 and other regulatory proteins, and a shorter C-terminal region with putative binding sites for additional regulatory proteins (Patterson et al., 2004; Foskett et al., 2007; Foskett, 2010). InsP_3Rs are usually located in the membrane of endoplasmic reticulum and vesicles, but are also found at low levels in the plasma membrane (Furuichi et al., 1989; Yule et al., 2010; Dellis et al., 2006; Taylor et al., 2009a; Taylor et al., 2009b; Barrera et al., 2007; Bezprozvanny, 2005; Delmas et al., 2002; Joseph, 1996; Tanimura et al., 2000; Tojyo et al., 2008; Rossier et al.,

1991; Fadool and Ache, 1994). In the endoplasmic reticulum, they play roles in Ca^{2+} homeostasis (Maeda et al., 1991; Ferris et al., 1989; Foskett et al., 2007). Deletion of the *iplA* gene in *D. discoideum* has been shown to block Ca^{2+} influx across the plasma membrane in response to a global cAMP signal (Traynor et al., 2000; Schaloske et al., 2005; Shanley et al., 2006). Mutant *iplA*$^{-}$ cells, however, were found to undergo chemotaxis in a spatial gradient of cAMP released from a micropipette, leading to the conclusion that Ca^{2+} influx stimulated by cAMP was not necessary for cAMP chemotaxis. It was subsequently discovered that *iplA*$^{-}$ cells lost shear-induced motility (i.e. mechanoreception) (Fache et al., 2005; Lombardi et al., 2008). Together, these results suggested that IplA was a strong candidate for a cell surface molecule or a molecule in the signal transduction pathway that mediated the facilitating effects of extracellular Ca^{2+} on motility and cAMP chemotaxis, and/or Ca^{2+} chemotaxis (Lusche et al., 2009; Scherer et al., 2010).

Here, we provide evidence that IplA plays selective roles in the extracellular effects of Ca^{2+} on cell behavior. It is necessary for Ca^{2+} facilitation of increased velocity, but not for the increases caused by the alternative cation K^{+}. More interestingly, IplA is essential for chemotaxis in a spatial gradient of Ca^{2+}, but not for chemotaxis in a spatial gradient of cAMP. It is also not essential for the chemokinetic responses to temporal waves of cAMP that mimic the temporal dynamics of natural cAMP waves. Given that *iplA*$^{-}$ cells chemotax normally in spatial gradients of cAMP generated in vitro and exhibit normal chemokinetic responses to temporal waves of cAMP generated in vitro, we fully expected *iplA*$^{-}$ cells to behave normally to natural waves of cAMP generated in an aggregation territory. This was based on the assumption that the complete behavior of amoebae in natural aggregation territory could be explained by their behavior in spatial and temporal gradients of cAMP. Instead, we found that although *iplA*$^{-}$ cells undergo a normal chemokinetic surge in velocity in response to the increasing phase of each naturally relayed cAMP wave in wild-type aggregation territories, they lose the ability to reorient towards the aggregation center at the onset of the front of each wave. These results support a hypothesis, previously entertained (Scherer et al., 2010), that transient Ca^{2+} gradients might be generated between cells at the onset of the front of each natural relayed cAMP wave that augment orientation towards the center of an aggregation territory, the source of each wave. If this hypothesis proves to be true, it would provide a more complex context for interpreting mutations that affect natural chemotaxis.

Results

IplA localization

In *D. discoideum*, IplA, a presumed Ca^{2+} channel, contains six transmembrane domains (Fig. 1A) (Traynor et al., 2000). The loop that includes the membrane spanning regions 5 and 6 has been shown in human IplAs to include the Ca^{2+} transport (pore) domain (Fig. 1A) (Ramos-Franko et al., 1999; da Fonseca et al., 2003). Models generated for the human IplA ortholog suggest that the N- and C-terminal regions are probably cytoplasmic, whether in the membrane of the endoplasmic reticulum or the plasma membrane (Fig. 1A) (Foskett et al., 2007; Foskett, 2010). To assess the localization of IplA, we generated the mutant strain *iplA*$^{-}$ complemented with a plasmid in which wild-type *iplA*$^{+}$ was linked to GFP, *iplA*$^{-}$/*iplA*$^{+}$-GFP. The *iplA*$^{+}$-GFP construct was under the regulation of the actin promoter. In living *iplA*$^{-}$/*iplA*$^{+}$-GFP cells, IplA–GFP localized in vesicles throughout the cytoplasm (Fig. 1E–H). These vesicles also abutted the plasma membrane. When brightness was enhanced to assess plasma membrane localization, the increased brightness of the associated vesicles precluded visualization of low plasma membrane fluorescence. To visualize membranes, we isolated plasmid membrane ghosts by Triton extraction according to the methods of Condeelis (Condeelis, 1979). Image enhancement revealed fluorescence in the plasma membranes (Fig. 1K–N). Membranes from *iplA*$^{-}$ cells analyzed similarly exhibited no autofluorescence (Fig. 1I,J). A control strain was generated in the *iplA*$^{-}$ background in which only the GFP gene was placed under the regulation of the actin promoter. Fluorescence of GFP in strain *iplA*$^{-}$-GFP was diffuse throughout the cytoplasm of living cells (supplementary material Fig. S1) and not associated with the plasma membrane. Together, these results indicate that IplA is localized primarily in vesicular membranes in the cytoplasm and suggest low levels in the plasma membrane.

Ca^{2+} binding

To test whether IplA plays a role in Ca^{2+} binding at the cell surface, cells were treated with NaN_3 for 30 minutes, which inhibits Ca^{2+} transport, and then incubated with $^{45}Ca^{2+}$ for 5 minutes (Wick et al., 1978; Milne and Coukell, 1991; Milne and Devreotes, 1993; Groner and Malchow, 1996). In three separate experiments, *iplA*$^{-}$ cells exhibited respective decreases in Ca^{2+} binding to 73, 61 and 64% that of control cells, suggesting that at least a portion of Ca^{2+} binding to the plasma membrane is mediated by IplA (Fig. 1B).

Behavioral assays

To test for selective Ca^{2+}-dependent defects in the *iplA*$^{-}$ mutant, we employed three chambers (Fig. 2). The Sykes–Moore chamber (Fig. 2A) is round with upper and lower glass walls, and a metal clamped rim with inlet and outlet ports. The ports are attached to pumps (Varnum et al., 1985; Varnum-Finney et al., 1987; Varnum-Finney et al., 1988), allowing perfusion with buffer in order to assess basic cell motility in the absence of cAMP. This chamber can also be used to assess behavior in response to temporal waves of cAMP, generated by a pump system. These waves mimic the temporal dynamics of a series of natural cAMP waves, without establishing spatial gradients of cAMP (Varnum et al., 1985; Varnum-Finney et al., 1987; Wessels and Soll, 1990; Wessels et al., 1992; Wessels et al., 2009).

However, because the Sykes–Moore chamber is round, it generates randomly directed shear forces that can affect the behavior of cells by activating IplA, a putative mechanoreceptor (Fache et al., 2005; Lombardi et al., 2008). The Zigmond chamber (Fig. 2B) consists of a bridge, which supports cells, bordered by two wells (Zigmond, 1977; Varnum and Soll, 1984). If one well is filled with buffer alone (‘sink’) and the other with buffer plus cAMP (‘source’), a cAMP gradient is generated across the bridge and chemotaxis can then be assessed at the single cell level. If both wells are filled with the same buffer solution lacking cAMP, basic motile behavior can be assessed at low cell density in the absence of shear forces. Although the Zigmond chamber is effective in assessing chemotaxis in a spatial gradient of cAMP, it is ineffective in assessing Ca^{2+} chemotaxis, given that Ca^{2+} gradients rapidly dissipate because of the high diffusion rate of the cation. To test for Ca^{2+}

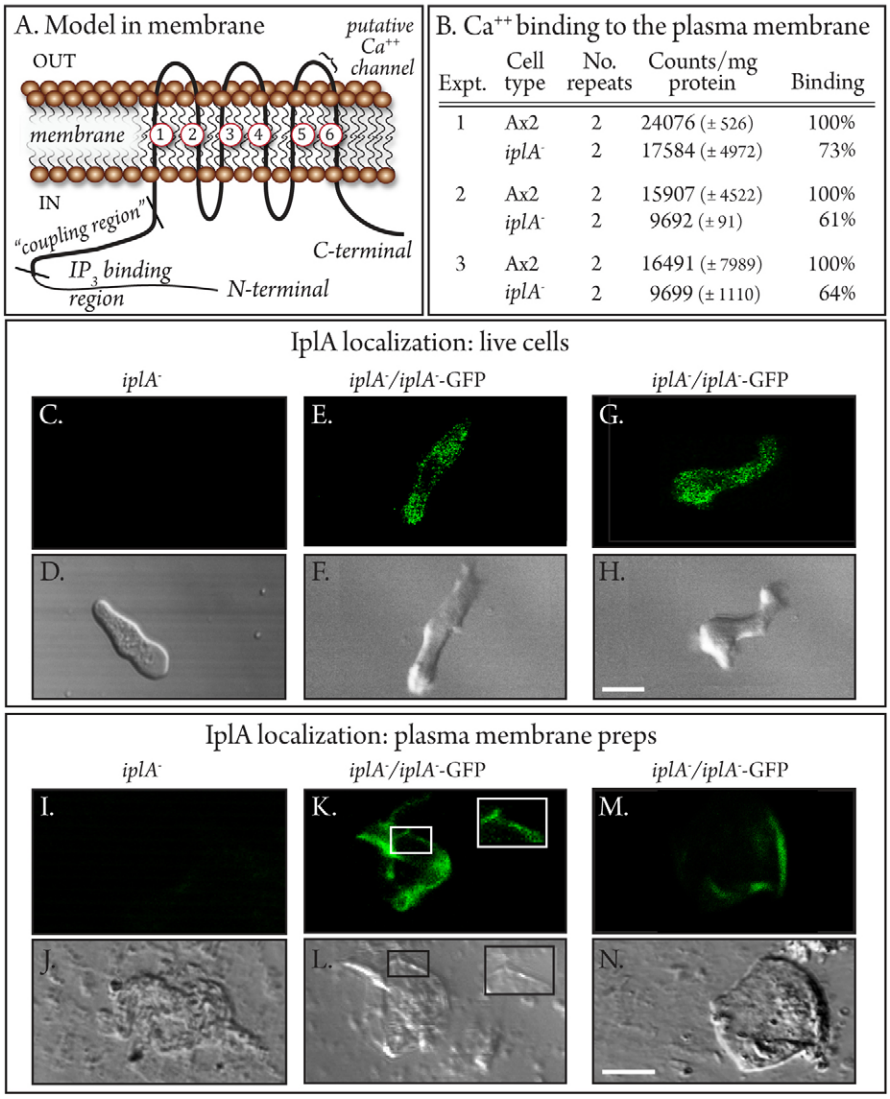

Fig. 1. IplA, a putative Ca^{2+} channel, containing six transmembrane domains, is involved in Ca^{2+} binding and is distributed at high levels in cytoplasmic vesicles and very low levels in the plasma membrane. (**A**) A general model for IplA in a membrane, based on models developed for inositol trisphosphate receptors in higher eukaryotes (Furuichi et al., 1989; Joseph, 1996; Foskett et al., 2007; Foskett, 2010; Mignery and Sudhof, 1990). IP_3, inositol trisphosphate. (**B**) The *iplA*$^-$ mutant binds less extracellular $^{45}Ca^{2+}$ than parental Ax2 cells. (**C**,**D**) Fluorescence and differential interference contrast microscopy (DIC) images, respectively, of a representative live *iplA*$^-$ cell, showing no fluorescence. (**E**–**H**) Fluorescence (E,G) and DIC (D,H) images of two live *iplA*$^-$/*iplA*$^+$-GFP cells, showing vesicular staining throughout the cytoplasm. (**I**,**J**) Fluorescence and DIC images, respectively, of a representative *iplA*$^-$ plasma membrane ghost, showing no fluorescence upon image enhancement. (**K**–**N**) Fluorescent (K,M) and DIC (L,N) images of representative *iplA*$^-$/*iplA*$^+$-GFP plasma membrane ghosts, showing low-level fluorescence upon image enhancement. Note that the fluorescence of whole live cells was far higher than that of the plasma membrane, and that the *iplA*$^-$ images were taken with the same settings or with the same enhancement as *iplA*$^-$/*iplA*$^+$-GFP images. Scale bar: 5 µm.

chemotaxis, we designed a microfluidic chamber that generates stable Ca^{2+} gradients (Fig. 2C) (Scherer et al., 2010). Although this chamber can be used to assess chemotaxis in spatial gradients of Ca^{2+} or cAMP, it produces strong shear forces, which can effect flow-directed movement (Scherer et al., 2010).

Behavior of *iplA*$^-$ cells in the absence of cAMP

As we previously reported for parental Ax2 cells (Lusche et al., 2009; Lusche et al., 2011), increasing the concentration of Ca^{2+} in Tricine buffer (TB) from 5 to 10 mM, in the absence of cAMP, resulted in dramatic increases in the three measured cell motility parameters: instantaneous velocity (Fig. 3A,B), the proportion of cells with instantaneous velocities of ≥9 µm/minute (Fig. 3A,C) and positive flow (Fig. 3A,D). All of these increases proved statistically significant ($P=7.0\times10^{-7}$, 6.0×10^{-5} and 4.0×10^{-7}; supplementary material Table S1). And as previously reported (Lusche et al., 2009; Lusche et al., 2011), increasing the Ca^{2+} concentration in TB from 0 to 5 mM in the

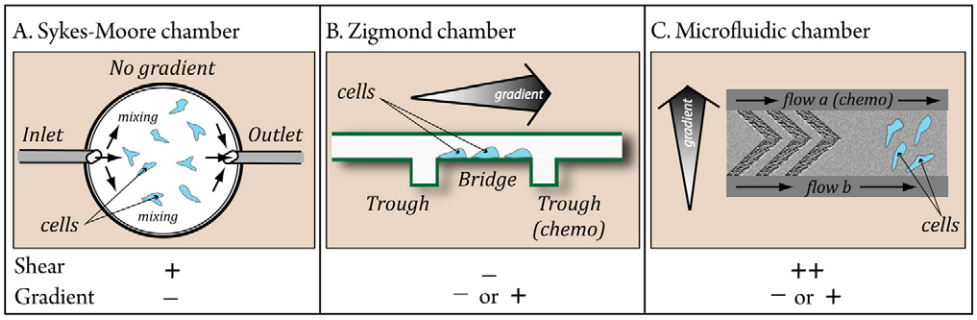

Fig. 2. Three different chambers were used to assess cell behavior. (**A**) The Sykes–Moore chamber. (**B**) The Zigmond gradient chamber. (**C**) The microfluidic chamber. Chambers are described in the Results section. Shear force and the capacity to generate a chemotactic gradient are noted at the bottom of panels.

A. Motility parameters

[Ca++]	Cell type	Cell no.	Inst. vel. (μm/min)	≥ 9 μm/min	Pos. flow (%/4sec)	Direct. persist.	Mot. cells
0 mM	Ax2	39	6.3 (± 2.7)	9%	9.8 (± 2.4)	0.27 (± 0.21)	82%
	iplA⁻	31	5.4 (± 2.0)	14%	8.1 (± 2.9)	0.25 (± 0.21)	58%
	iplA⁻/*iplA*⁺	48	6.7 (± 2.7)	12%	6.3 (± 1.6)	0.38 (± 0.19)	69%
5 mM	Ax2	79	7.5 (± 4.1)	29%	9.1 (± 3.4)	0.39 (± 0.21)	86%
	iplA⁻	54	7.3 (± 2.8)	32%	9.8 (± 3.1)	0.27 (± 0.28)	83%
10 mM	Ax2	33	12.9 (± 5.7)	68%	14.1 (± 4.7)	0.40 (± 0.21)	94%
	iplA⁻	54	7.5 (± 4.1)	35%	9.8 (± 5.1)	0.44 (± 0.22)	79%
	iplA⁻/*iplA*⁺	52	12.2 (± 4.4)	79%	13.3 (± 3.6)	0.58 (± 0.24)	98%

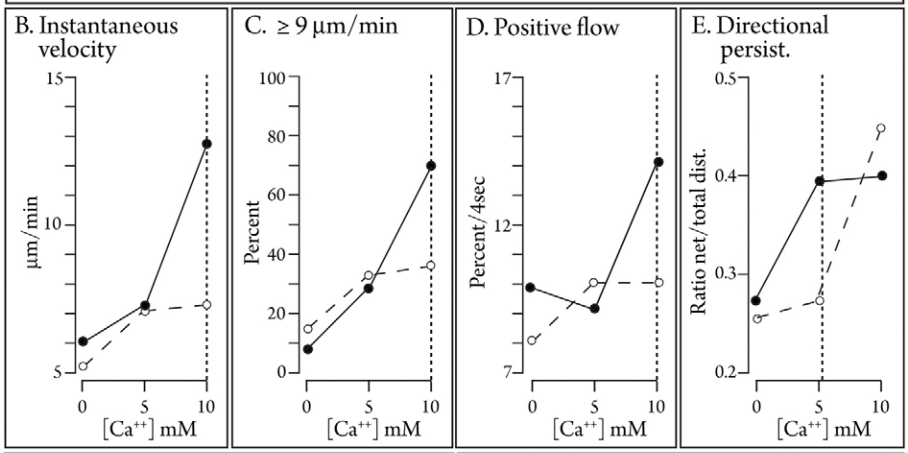

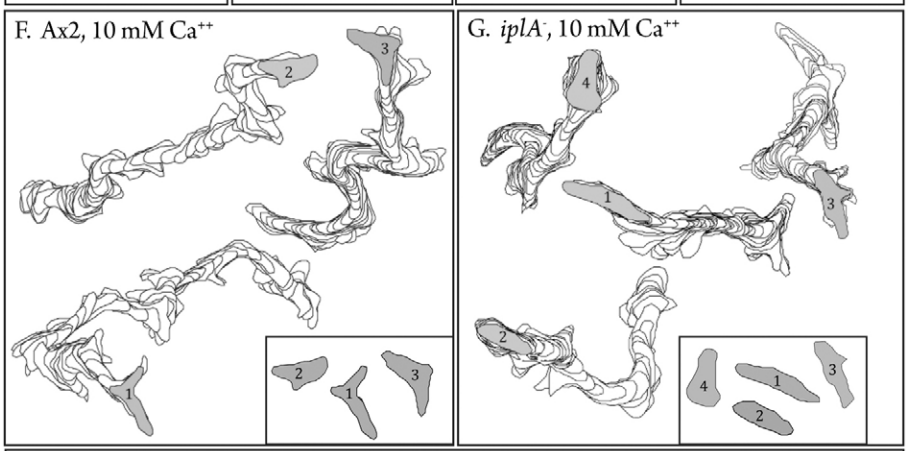

H. Motility parameters

[K⁺]	Cell type	Cell no.	Inst. vel. (μm/min)	≥ 9 μm/min	Pos. flow (%/4sec)	Direct. persist.	Mot. cells
40 mM	Ax2	55	7.7 (± 3.7)	32%	7.2 (± 2.3)	0.33 (± 0.15)	75%
	iplA⁻	127	7.3 (± 3.9)	20%	7.3 (± 2.3)	0.32 (± 0.20)	77%

Fig. 3. Mutant *iplA*⁻ cells exhibit selective defects in the facilitation of velocity by Ca^{2+}. The behavior of mutant *iplA*⁻ cells was compared with that of parental Ax2 and complemented *iplA*⁻/*iplA*⁺ cells in a Sykes–Moore chamber perfused with TB containing different concentrations of Ca^{2+}, in the absence of cAMP. (**A**) Motility parameters (means ± standard deviation) at different concentrations of Ca^{2+}. (**B**) Instantaneous velocity plotted as a function of Ca^{2+} concentration. (**C**) Proportion of cells with instantaneous velocities ≥9 μm/minute plotted as a function of Ca^{2+} concentration. (**D**) Positive flow plotted as a function of Ca^{2+} concentration. (**E**) Directional persistence plotted as a function of Ca^{2+} concentration. (**F**,**G**) Perimeter tracks of representative parental Ax2 and *iplA*⁻ cells, respectively, translocating in TB containing 10 mM Ca^{2+}. Insets in F and G reveal no differences in shape. (**H**) Motility parameters of Ax2 and *iplA*⁻ cells in a Sykes–Moore chamber perfused with TB containing 40 mM K^+ in the absence of cAMP.

absence of cAMP resulted in an increase in the directional persistence of translocating cells (Fig. 3A,E) that was statistically significant ($P=5.0\times10^{-3}$; supplementary material Table S1). Mutant *iplA*⁻ cells did not show increases in velocity parameters comparable with the increases in wild-type cells when the Ca^{2+} concentration in TB was increased to 10 mM (Fig. 3A–D). Mutant *iplA*⁻ also did not undergo an increase in directional persistence when the Ca^{2+} concentration was increased from 0 to 5 mM, although they did undergo the increase when the Ca^{2+} concentration was increased to 10 mM (Fig. 3A,E). The defects in responsiveness of *iplA*⁻ cells to 10 mM Ca^{2+} were discernible in computer-generated perimeter tracks. The tracks of *iplA*⁻ cells (Fig. 3G) were on average more contracted than those of Ax2 cells (Fig. 3F). No major differences in cell shape were evident (see inserts in Fig. 3F,G).

If IplA plays a selective role in the cationic facilitation of cell motility by Ca^{2+} in the absence of cAMP, then cells of the null mutant *iplA*⁻ and its parent strain Ax2 should exhibit no behavioral differences from wild-type cells when translocating in TB containing 40 mM K^+, the facilitating concentration of this monovalent cation in the absence of added Ca^{2+} (Lusche et al., 2009). This prediction is predicated on the discovery that K^+, but not Ca^{2+}, facilitation is mediated by Nhe1 (Lusche et al., 2011). When perfused with a 40 mM K^+ solution in a Sykes–Moore

chamber, all motility parameters were similar in *iplA*$^{-}$ and wild-type cells (Fig. 3H), supporting the conclusion that in the absence of cAMP, K^{+} facilitation is mediated by Nhe1, not IplA and that Ca^{2+} facilitation is mediated by IplA, not Nhe1.

Motility and chemotactic orientation in a spatial gradient of cAMP

As we previously reported for parental Ax2 cells (Lusche et al., 2009), increasing the concentration of Ca^{2+} in TB to 10 mM in a spatial gradient of cAMP caused an increase in the three motility parameters, instantaneous velocity (Fig. 4A,B), percentage of cells with instantaneous velocities of ≥9 μm/minute (Fig. 4A,C), and positive flow (Fig. 4A). Increasing the concentration from 0 to 5 mM caused an increase in directional persistence (Fig. 4A,D). In the case of *iplA*$^{-}$ cells in a spatial gradient of cAMP, there were less pronounced increases in the velocity parameters (Fig. 1A–C). Directional persistence, however, increased at 5 mM, as it did in Ax2 cells (Fig. 4A,D). The differences between *iplA*$^{-}$ and Ax2 cells were either less pronounced or negligible in a spatial gradient of cAMP than in the absence of cAMP (Fig. 3; supplementary material Table S1). Only the differences in instantaneous velocity and percentage of cells with instantaneous velocities of ≥9 μm/minute were significant ($P=5.0\times10^{-3}$, 4.0×10^{-3}; supplementary material Table S1). These results are consistent with previous observations, especially on lateral pseudopodium formation and turning, indicating that a spatial gradient of cAMP enhances the effect of Ca^{2+} (Lusche et al., 2009).

As previously reported (Lusche et al., 2009; Lusche et al., 2011; Scherer et al., 2010), when Ca^{2+} was not added (0 mM Ca^{2+}) to a spatial gradient of cAMP generated in TB, Ax2 cells still underwent chemotaxis, but with a reduced chemotactic index

A. Motility parameters

[Ca^{++}]	Cell type	Cell no.	Inst. vel. (μm/min)	≥ 9 μm/min	Pos. flow (%/4sec)	Direct. persist.	Chem. index	Pos. chem.	Mot. cells
0 mM	Ax2	46	6.0 (± 1.7)	7%	7.0 (± 2.1)	0.57 (± 0.26)	+0.34 (± 0.35)	80%	83%
	iplA^{-}	52	6.1 (± 2.3)	7%	8.3 (± 2.2)	0.33 (± 0.20)	+0.01 (± 0.30)	70%	79%
	iplA^{-}/*iplA*$^{+}$	33	6.1 (± 2.8)	12%	10.7 (± 2.1)	0.49 (± 0.21)	+0.21 (± 0.35)	84%	75%
5 mM	Ax2	66	7.1 (± 2.9)	21%	5.9 (± 1.6)	0.76 (± 0.21)	+0.69 (± 0.21)	98%	89%
	iplA^{-}	26	6.3 (± 2.5)	20%	5.8 (± 1.4)	0.76 (± 0.14)	+0.75 (± 0.14)	100%	81%
10 mM	Ax2	40	10.5 (± 2.5)	82%	10.1 (± 4.3)	0.77 (± 0.19)	+0.74 (± 0.19)	100%	97%
	iplA^{-}	31	8.3 (± 3.2)	45%	9.1 (± 2.9)	0.60 (± 0.17)	+0.59 (± 0.16)	96%	79%
	iplA^{-}/*iplA*$^{+}$	25	9.4 (± 2.2)	62%	11.0 (± 2.5)	0.74 (± 0.16)	+0.69 (± 0.17)	100%	85%

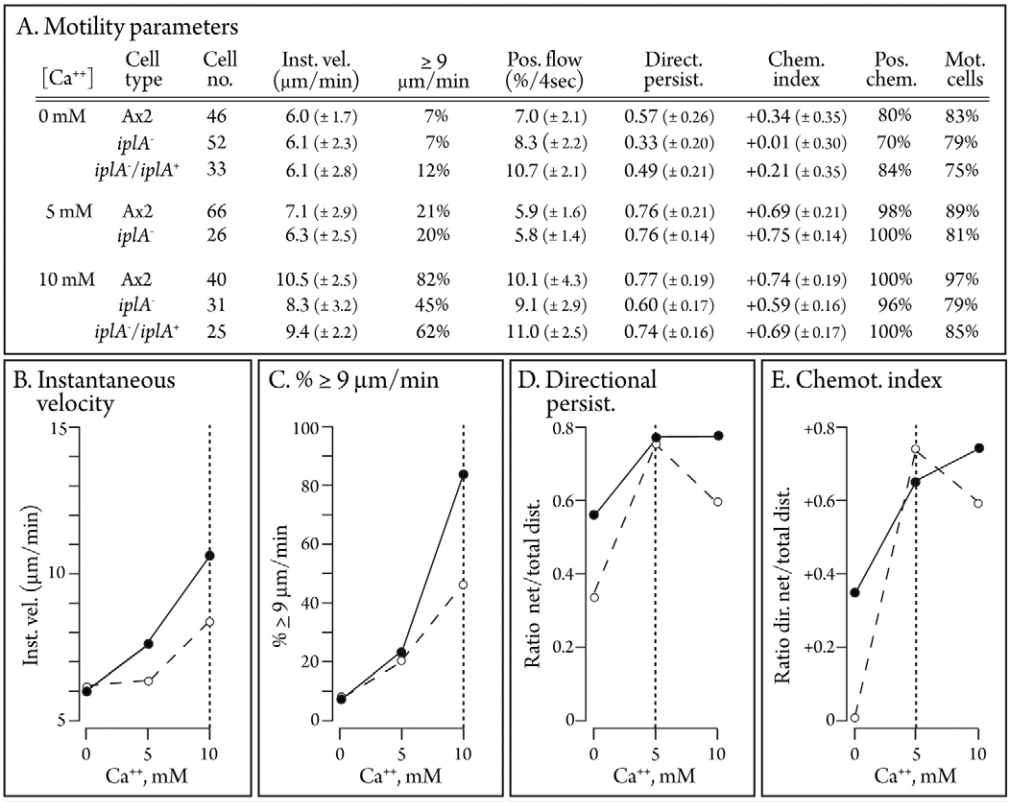

H. Motility parameters

[K^{+}]	Cell type	Cell no.	Inst. vel. (μm/min)	≥ 9 μm/min	Pos. flow (%/4sec)	Direct. persist.	Chem. index	Pos. chem.	Mot. cells
40 mM	Ax2	34	9.0 (± 3.4)	60%	7.6 (± 2.6)	0.71 (± 0.15)	+0.69 (± 0.15)	100%	71%
	iplA^{-}	28	8.7 (± 3.6)	48%	7.1 (± 1.4)	0.77 (± 0.21)	+0.71 (± 0.34)	95%	79%

Fig. 4. Mutant *iplA*$^{-}$ cells exhibit selective defects in Ca^{2+} facilitation of velocity, but undergo normal chemotaxis in a spatial gradient of cAMP. Studies were performed in spatial gradients of cAMP generated in TB containing different Ca^{2+} concentrations in a Zigmond chamber. (**A**) Motility parameters (means ± standard deviation) at different concentrations of Ca^{2+}. (**B**) Instantaneous velocity as a function of Ca^{2+} concentration. (**C**) Proportion of cells with instantaneous velocities ≥9 μm/minute as a function of Ca^{2+} concentration. (**D**) Directional persistence as a function of time. (**E**) Chemotactic index as a function of time. (**F**,**G**) Perimeter tracks of Ax2 and *iplA*$^{-}$ cells, respectively, in cAMP gradients generated in 10 mM Ca^{2+}. Insets are for shape comparisons. (**H**) Motility parameters of Ax2 and *iplA*$^{-}$ in spatial gradients generated in TB containing 40 mM K^{+} in TB.

(CI) of 0.34±0.35 and a percentage positive chemotaxis value of 80% (Fig. 4A,E). Also, as previously reported (Lusche et al., 2009; Lusche et al., 2011), Ax2 cells attained maximum chemotactic orientation (CI=+0.69±0.21; percentage positive chemotaxis=98%) when the Ca^{2+} concentration was raised to 5 mM (Fig. 4A,E) (Lusche et al., 2009; Lusche et al., 2011; Scherer et al., 2010). Although relatively mobile, *iplA*$^{-}$ cells exhibited negligible chemotactic orientation (CI=+0.01±0.30; percentage positive chemotaxis=70%) in a spatial gradient of cAMP at 0 mM Ca^{2+}, but exhibited maximum chemotactic orientation (CI=+0.75±0.14), similar to that of Ax2 cells, when the concentration of Ca^{2+} was raised to 5 mM (Fig. 4A,E). The relatively high efficiency of chemotaxis by *iplA*$^{-}$ cells in a spatial gradient of cAMP generated in TB containing 10 mM Ca^{2+} was evident in representative perimeter tracks (Fig. 4F,G). These results support the earlier observations by Traynor et al. (Traynor et al., 2000). They also indicate that as is the case for Ax2 cells, chemotactic orientation of *iplA*$^{-}$ cells in a nonfacilitating concentration of K^{+} or Na^{+} requires 5 mM Ca^{2+}, and this latter requirement is independent of IplA.

If IplA functions specifically in the facilitation of maximum velocity, then the *iplA*$^{-}$ and Ax2 cells should exhibit similar maximum motility and chemotactic orientation in a spatial gradient of cAMP generated in TB containing 40 mM K^{+}. When a spatial gradient of cAMP was generated in TB containing 40 mM K^{+} with no added Ca^{2+}, the motility and chemotaxis parameters of *iplA*$^{-}$ cells were similar for Ax2 and *iplA*$^{-}$ cells (Fig. 4H).

Responses to temporal gradients of cAMP

In a naturally aggregating population of *D. discoideum* cells the pulses of cAMP released from cells at an aggregation center (Gerisch et al., 1966; Konijn et al., 1967; Devreotes and Steck, 1979) are relayed through the population as outwardly moving, nondissipating, symmetrical waves (Tomchik and Devreotes, 1981; Devreotes et al., 1983). In the front of each wave, an amoeba experiences an increasing temporal as well as an increasing spatial gradient of cAMP and in the back of each wave, it experiences a decreasing temporal as well as a decreasing spatial gradient of cAMP (Soll et al., 2002). At the peak and in the back of each wave, amoebae undergo a decrease polarity and directionality, and a dramatic decrease in velocity (Varnum et al., 1985; Wessels et al., 1992; Soll et al., 2002). At the onset of the front of next relayed wave, an amoeba reorients towards the aggregation center, and then moves in a rapid and persistent fashion towards the aggregation center, in what appears to be a relatively semi-blind fashion in response to the increasing temporal gradient of cAMP, which serves as chemokinetic signal (Wessels et al., 1992; Soll et al., 2002). To test whether *iplA*$^{-}$ cells were capable of assessing the temporal dynamics of a wave, we challenged them with a series of four temporal waves generated in buffered salt solution with K^{+} as the facilitating cation. The waves were generated in the absence of an established spatial gradient in a Sykes–Moore chamber (Fig. 2A) attached to a pump system (Varnum et al., 1985; Wessels et al., 1992). Mutant *iplA*$^{-}$ cells underwent a transient increase in velocity in the increasing phase, and a decrease at the peak and in the decreasing phase, of a majority of the temporal cAMP waves (Fig. 5C,D), in a manner similar to that of parental Ax2 cells (Fig. 5A,B). Ten additional Ax2 and 10 additional *iplA*$^{-}$ cells responded in a similar fashion. Therefore, chemokinetic responsiveness to the increasing phases of cAMP waves generated in vitro, as well as chemotactic orientation in a spatial gradient of cAMP generated in vitro, are intact in *iplA*$^{-}$ cells (Fig. 4).

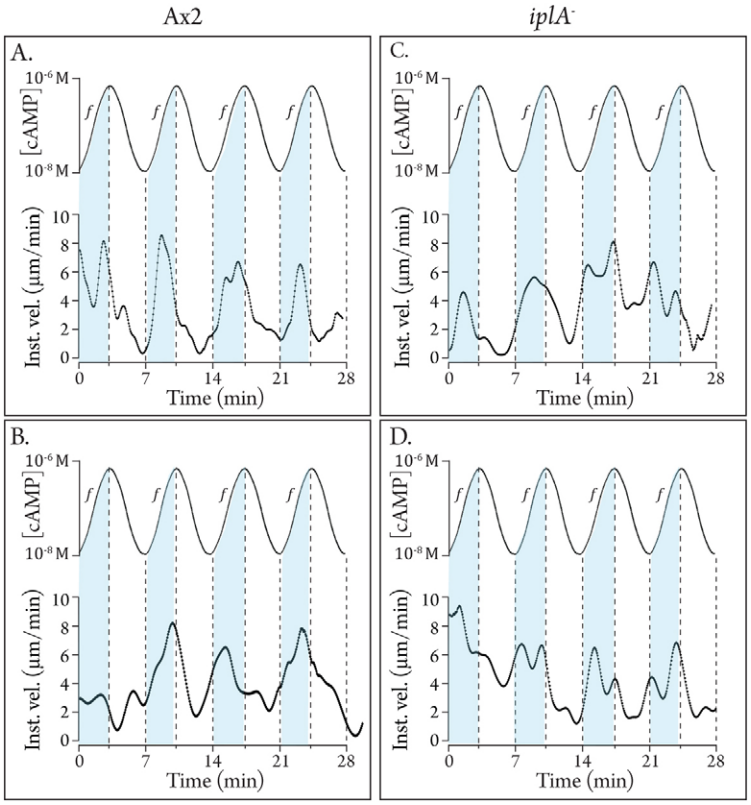

Fig. 5. Mutant *iplA*$^{-}$ cells undergo increases in instantaneous velocity in the increasing phase (f, blue zone) of a series of temporal waves of cAMP generated in a Sykes–Moor chamber. The temporal waves of cAMP approximate the temporal dynamics of natural cAMP waves in the absence of a spatial gradient. These experiments were performed in a buffered salt solution containing 40 mM K^{+} as the facilitating cation.

Ca^{2+} chemotaxis is lost in *iplA*$^{-}$ cells

To test for Ca^{2+} chemotaxis, a microfluidic chamber was employed (Fig. 2C) in which stable Ca^{2+} gradients were established (Scherer et al., 2010). We first compared the behavior of Ax2 and *iplA*$^{-}$ cells in the chamber in uniform 10 mM Ca^{2+}. The parameter 'rightward directionality' (RD), movement in the direction of flow (shear force), was computed as the net distance traveled rightward (x) divided by the total distance traveled (y; Fig. 6A). An RD of +1.00 represents absolute rightward directionality, an RD of 0.00 represents random directionality, and an increasing positive RD, from +0.01 to +0.99, reflects increasing rightward directionality. At a global concentration of 10 mM Ca^{2+}, in the absence of a Ca^{2+} gradient, the mean instantaneous velocity of *iplA*$^{-}$ cells was 6.0±2.6 μm/minute, compared with 10.9±5.3 μm/minute for Ax2 cells, a reduction of 45% (Fig. 6D). The proportion of *iplA*$^{-}$ cells with instantaneous velocities ≥9 μm/minute was also well below that of Ax2 cells (Fig. 6D). The RD of Ax2 cells was +0.59±0.34, whereas the RD of *iplA*$^{-}$ cells was close to 0.00 (+0.04±0.27; Fig. 6D). The percentage of Ax2 cells exhibiting rightward movement was 87%, whereas that of *iplA*$^{-}$ cells was close to 50%, demonstrating that the direction of *iplA*$^{-}$ cells under strong

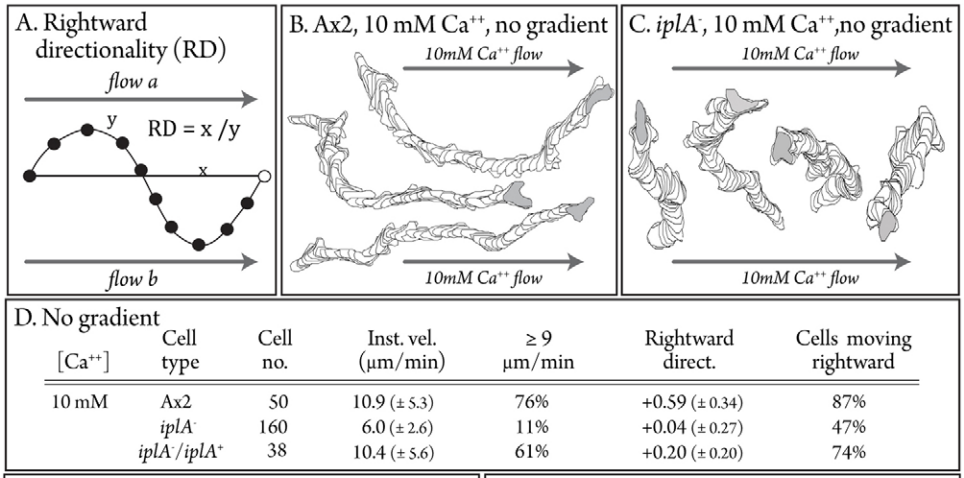

D. No gradient

[Ca^{++}]	Cell type	Cell no.	Inst. vel. (μm/min)	≥ 9 μm/min	Rightward direct.	Cells moving rightward
10 mM	Ax2	50	10.9 (± 5.3)	76%	+0.59 (± 0.34)	87%
	iplA^{-}	160	6.0 (± 2.6)	11%	+0.04 (± 0.27)	47%
	iplA^{-}/*iplA*$^{+}$	38	10.4 (± 5.6)	61%	+0.20 (± 0.20)	74%

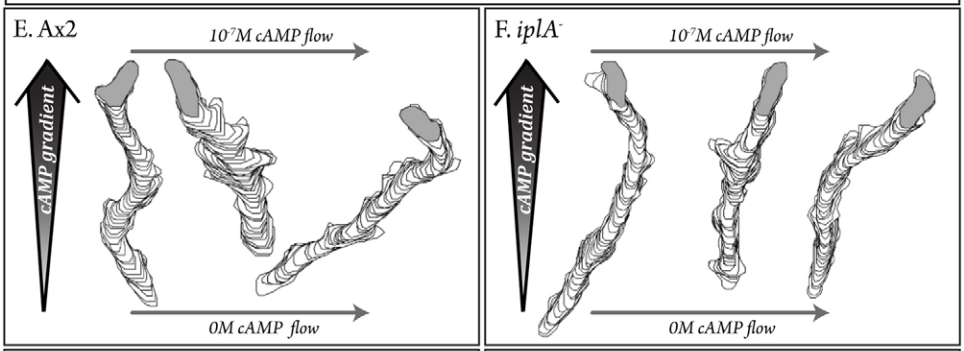

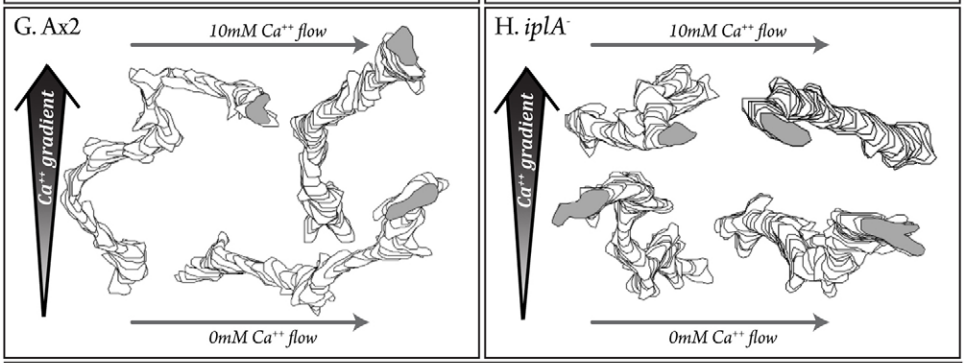

I. Gradients

Gradient	Cell type	Cell no.	Inst. vel. (μm/min)	Rightward direct.	Chem. index	Pos. chem.
cAMP	Ax2	108	6.0 (± 2.9)	+0.09 (± 0.31)	+0.35 (± 0.35)	90%
	iplA^{-}	64	7.5 (± 2.9)	-0.05 (± 0.34)	+0.30 (± 0.30)	84%
Ca^{++}	Ax2	68	10.5 (± 2.9)	+0.25 (± 0.38)	+0.20 (± 0.25)	86%
	iplA^{-}	135	7.1 (± 3.6)	- 0.04 (± 0.33)	+0.01 (± 0.29)	49%
	iplA^{-}/*iplA*$^{+}$	18	10.4 (± 5.6)	+0.10 (± 0.30)	+0.26 (± 0.24)	83%

Fig. 6. Mutant *iplA*$^{-}$ cells lose the capacity to undergo chemotaxis in a spatial gradient of Ca^{2+} generated in a microfluidic chamber. (**A**) Computing rightward directionality (RD). *x*, net distance a cell moves to the right, the direction of flow; *y*, total distance a cell moves. (**B**) Rightward movement of representative parental Ax2 cells in response to the rightward shear force in the absence of a chemotactic gradient, in uniform 10 mM Ca^{2+} in TB. (**C**) The absence of rightward movement of representative mutant *iplA*$^{-}$ cells in response to rightward shear force in the absence of a chemotactic gradient in uniform 10 mM Ca^{2+}. (**D**) Motility parameters in the absence of a chemotactic gradient in the microfluidic chamber in uniform 10 mM Ca^{2+} in TB. (**E**) Chemotaxis up a cAMP gradient by parental Ax2 cells. The cAMP gradient was generated in 10 mM Ca^{2+} in TB. (**F**) Chemotaxis up a cAMP gradient by *iplA*$^{-}$ cells. The cAMP gradient was generated in 10 mM Ca^{2+} in TB. (**G**) Chemotaxis up a Ca^{2+} gradient by parental Ax2 cells. The Ca^{2+} gradient was generated in TB. (**H**) Random movement in a Ca^{2+} gradient by *iplA*$^{-}$ cells. The Ca^{2+} gradient was generated in TB. (**I**) Motility and chemotaxis parameters in a cAMP or Ca^{2+} gradient generated in a microfluidic chamber.

flow was random (Fig. 6D). The loss of flow-induced directional movement and submaximal velocity by *iplA*$^-$ cells (Fig. 6C) was apparent in a comparison of their perimeter tracks with those of Ax2 (Fig. 6B,C). Similar results for *iplA*$^-$ cells were obtained at 20 and 30 mM Ca^{2+} (data not shown). These defects were consistent with those previously reported using very different assays (Fache et al., 2005; Lombardi et al., 2008).

We then compared the behavior of *iplA*$^-$ and Ax2 cells in spatial gradients of cAMP generated in the microfluidic chamber (Fig. 2C). As previously demonstrated (Scherer et al., 2010), although Ax2 cells translocated in the direction of flow in the absence of a cAMP gradient, they translocated in the direction of increasing cAMP in a spatial gradient of cAMP, with almost no bias to the right due to the direction of flow (Fig. 6E,I). Mutant *iplA*$^-$ cells moved up spatial gradients of cAMP with the same directionality as Ax2 cells (Fig. 6E,F,I). The chemotactic indices of Ax2 and *iplA*$^-$ cells in cAMP gradients in the microfluidic chamber were $+0.35\pm0.35$ and $+0.30\pm0.30$, respectively, and the percentage positive chemotaxis 90 and 84%, respectively (Fig. 6I). These results reinforce those obtained with the Zigmond chamber (Fig. 4) and micropipette assays (Traynor et al., 2000), demonstrating again that chemotaxis in a spatial gradient of cAMP is intact in *iplA*$^-$ cells.

We next tested whether *iplA*$^-$ cells underwent chemotaxis in Ca^{2+} gradients generated in the microfluidic chamber (Fig. 2C). Parental Ax2 cells had a chemotactic index of $+0.20\pm0.25$, percent cells with a positive chemotactic index of 86% and an instantaneous velocity of 10.5 ± 2.9 μm/minute (Fig. 6I), values very close to those we reported previously (Scherer et al., 2010). The RD of Ax2 cells in a Ca^{2+} gradient was $+0.25\pm0.38$, showing rightward bias (Fig. 6I). The bias can be recognized in representative perimeter tracks of Ax2 cells in a Ca^{2+} gradient (Fig. 6G). In marked contrast, the chemotactic index of *iplA*$^-$ cells in similar Ca^{2+} gradients was $+0.01\pm0.29$, a value indicating the loss of Ca^{2+} chemotaxis (Fig. 6I). The percentage *iplA*$^-$ cells with a positive chemotactic index was 49% (Fig. 6I), close to 50%, the value for directional randomness. The differences between Ax2 and *iplA*$^-$ cells were statistically significant ($P=2\times10^{-6}$, 6×10^{-8}; supplementary material Table S1). We further tested a variety of Ca^{2+} gradients varying in shape and concentration range, but observed no Ca^{2+} chemotaxis (data not shown). The RD of *iplA*$^-$ cells was -0.04 ± 0.33, very close to 0.00, indicating again the loss of flow-induced directionality (Fig. 6I). These results demonstrate that although *iplA*$^-$ cells have fully retained the capacity to undergo positive chemotaxis in a spatial gradient of cAMP, they have lost the capacity to undergo chemotaxis in a spatial gradient of Ca^{2+}. The directional movement of Ax2 cells with a rightward bias in a spatial gradient of Ca^{2+} and the random movement of *iplA*$^-$ cells with no rightward bias are reflected in a comparison of representative perimeter tracks (Fig. 6G and 6H, respectively).

Complementation of *iplA*$^-$ rescues defective phenotype

To test for complementation, we generated strain *iplA*$^-$/*iplA*$^+$-GFP, in which *iplA*$^+$ was under the regulation of the actin promoter in a nonintegrating plasmid. The three velocity parameters, instantaneous velocity, the proportion of cells with instantaneous velocities of ≥9 μm/cell, and positive flow, returned to wild-type levels in 10 mM Ca^{2+} in the absence of cAMP (Fig. 3A) and the chemotactic and mechanoreception defects were also rescued (Fig. 6I). The rescued levels (Fig. 3A, Fig. 4A, Fig. 6I) were indistinguishable statistically from that of the wild-type parent strain, Ax2 (i.e. $P<0.05$). These results demonstrate that the defects of *iplA*$^-$ cells were the direct result of the deletion of *iplA*$^+$ and not a second site mutation.

Chemotaxis of *iplA*$^-$ cells in natural Ax2 aggregation territories

If chemotaxis in a natural aggregation territory is regulated solely by the spatial and temporal dynamics of relayed waves of cAMP, as we have previously argued (Soll et al., 2002), then *iplA*$^-$ cells should undergo normal chemotaxis in natural chemotactic waves generated by wild-type cells. This prediction is predicated on their normal responses to spatial and temporal gradients of cAMP assayed in vitro. To test this prediction, we analyzed the behavior of vitally stained minority *iplA*$^-$ cells seeded in majority wild-type cell aggregation territories (Wessels et al., 2000a; Wessels et al., 2000b; Wessels et al., 2004; Wessels et al., 2007; Heid et al., 2004; Stepanovic et al., 2005). Under these conditions, minority mutant cells are challenged with natural waves relayed by majority wild-type cells. Mutant *iplA*$^-$ cells were stained with DiI during growth, mixed with unlabeled Ax2 cells at a ratio of 1:9 and the mixture of cells allowed to undergo aggregation on a plastic surface in buffered salt solution (Sussman, 1987), in which K^+ was the facilitating cation (Lusche et al., 2011). In the carpet of mixed cells established on the plastic surface, precocious cells, which act as aggregation centers, release pulses of cAMP and these signals are then relayed through the population as nondissipating outwardly moving waves (Tomchik and Devreotes, 1981) (Fig. 7A,B). The relayed waves can be deduced from the behavior of majority, unlabeled Ax2 cells, which undergo transient increases in velocity towards the aggregation center in the front of each wave, and decreases at the peak and in the back of each wave (Wessels et al., 1992; Wessels et al., 2000a; Wessels et al., 2000b; Wessels et al., 2007; Heid et al., 2004; Stepanovic et al., 2005; Soll et al., 2002). The behavior of minority *iplA*$^-$ cells in relayed waves could then be assessed through comparison with the behavior of Ax2 cells located within a 30 μm radius, which were responding to the same relayed waves. As revealed in time plots of instantaneous velocity, Ax2 cells (black dot plots) surged towards the aggregation center in the deduced front of each successive wave for approximately 2.5 minutes (Fig. 7C,E). The time interval between waves was approximately 7 minute (Fig. 7C,E). Neighboring mutant *iplA*$^-$ cells (red dot plots) surged in a similar fashion in the front of the same successive waves (Fig. 7C,E). There was, however, a defect in *iplA*$^-$ cells discerned in centroid tracks. Whereas Ax2 cells (black dot tracks) made relatively constant net progress towards the aggregation center in the front of each successive wave (Fig. 7D,F), *iplA*$^-$ cells (red dot tracks) surged relatively in random directions in the front of waves, thus making less net progress towards the aggregation center (Fig. 7D,F). The *iplA*$^-$ cells making the most progress towards the aggregation center was used for comparison in experiment 1 (Fig. 7D) and experiment 2 (Fig. 7F). Similar results were obtained in three independent experiments.

To quantify the apparent defect in orientation, we measured the angle, in degrees, between the direction of the wave (a) and the net direction of translocation (b) of individual majority wild-type cells and minority mutant *iplA*$^-$ cells in the front of each of four to five successive cAMP waves generated by the majority Ax2 cells in natural aggregation territories. Net direction directly

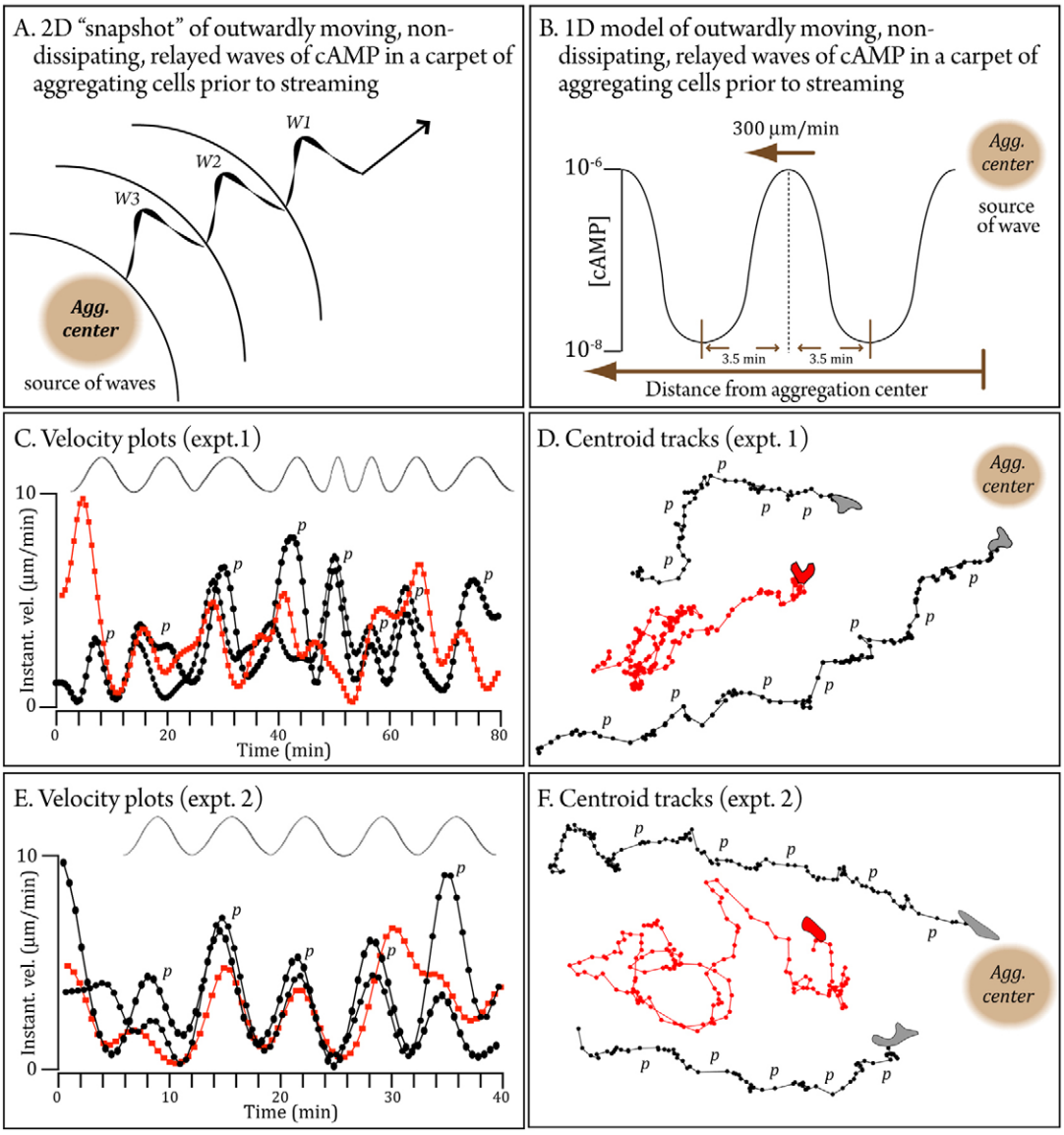

Fig. 7. Mutant *iplA*$^{-}$ cells do not reorient in the front of natural waves generated by parental Ax2 cells. To assess how *iplA*$^{-}$ cells respond to outwardly moving, nondissipating relayed waves of chemoattractant, DiI-labeled *iplA*$^{-}$ cells and unlabeled parental Ax2 cells were mixed in a 1:9 ratio and allowed to aggregate. Before streaming, the behavior of individual *iplA*$^{-}$ and Ax2 cells was analyzed. (**A**) 2D model of naturally relayed, outwardly moving, nondissipating waves of cAMP in an aggregation territory. (**B**) 1D model of naturally relayed waves. (**C**,**E**) Velocity plots from two independent experiments of individual majority parental Ax2 (black dots) and neighboring minority mutant *iplA*$^{-}$ (red dots) cells responding to natural waves. The waves diagrammed at top, were deduced from Ax2 cell behavior. (**D**,**F**) Centroid tracks from two independent experiments, of representative Ax2 cells (black dots) and *iplA*$^{-}$ cells (red dots). Agg. center, aggregation center. W1, W2, W3. Waves 1, 2 and 3. P, velocity peaks.

towards the aggregation center would be 0°, net direction directly away from the aggregation center would be 180°, and net random direction would be 90°. Models of a net angle (<) of translocation of 30° and 90° are presented in Fig. 8A and 8B, respectively. Although the mean angle of direction of the majority wild-type cells was 33±12°, that of minority *iplA*$^{-}$ cells was 101±22° (Fig. 8C), the latter close to the measure of randomness (i.e. 90°). These results demonstrate that even though *iplA*$^{-}$ cells can chemotax up a spatial gradient of cAMP generated in vitro, and even though they correctly surge in the increasing phase of temporal waves generated in vitro, they are impaired in their capacity to reorient correctly and move in the front of each natural cAMP wave in a directed fashion towards the source of a natural, relayed waves (i.e. the aggregation center).

Discussion

Following cloning of the first InsP_3R over 20 years ago from the mouse cerebellum (Furuichi et al., 1989), numerous inositol trisphosphate receptor genes have been identified and grouped into a family of transient receptor potential (TRP) channels (Vannier et al., 1998; Blondel et al., 1993; Maranto, 1994; Ross et al., 1992; Sudhof et al., 1991). Although most commonly found in the endoplasmic reticulum (Furuichi et al., 1989; Yule, et al., 2010), InsP_3Rs have also been found associated with the

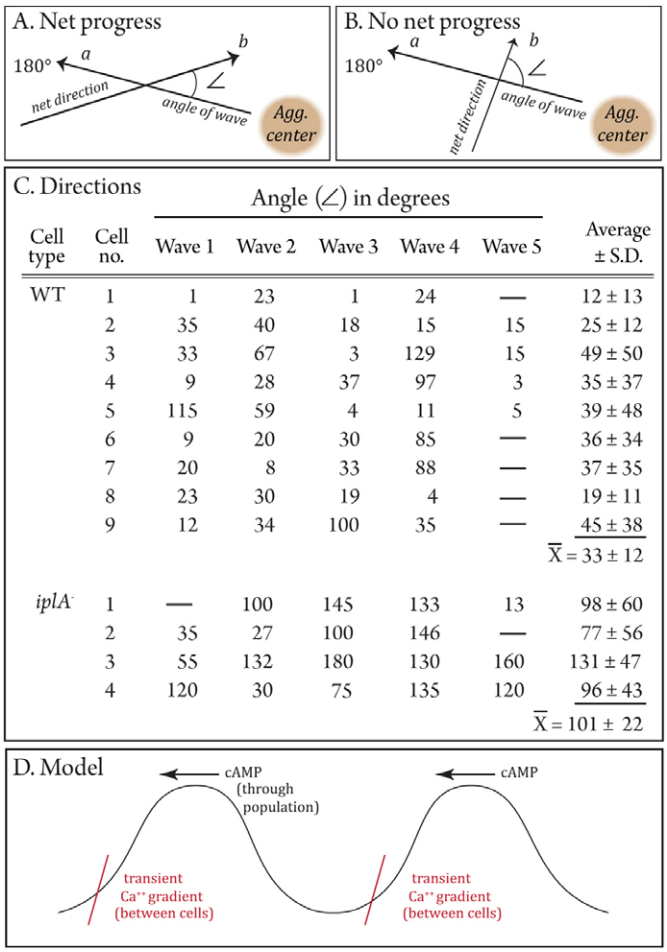

C. Directions

Cell type	Cell no.	Angle (∠) in degrees: Wave 1	Wave 2	Wave 3	Wave 4	Wave 5	Average ± S.D.
WT	1	1	23	1	24	—	12 ± 13
	2	35	40	18	15	15	25 ± 12
	3	33	67	3	129	15	49 ± 50
	4	9	28	37	97	3	35 ± 37
	5	115	59	4	11	5	39 ± 48
	6	9	20	30	85	—	36 ± 34
	7	20	8	33	88	—	37 ± 35
	8	23	30	19	4	—	19 ± 11
	9	12	34	100	35	—	45 ± 38
							$\bar{X}$ = 33 ± 12
iplA⁻	1	—	100	145	133	13	98 ± 60
	2	35	27	100	146	—	77 ± 56
	3	55	132	180	130	160	131 ± 47
	4	120	30	75	135	120	96 ± 43
							$\bar{X}$ = 101 ± 22

Fig. 8. Measurements of defective reorientation in the front of natural chemotactic waves. Mutant *iplA*⁻ cells and parental Ax2 cells were mixed at a 1:9 ratio and allowed to aggregate. Orientation angles (<) were computed in the front of each relayed wave. (**A**,**B**) Method for measuring orientation angle. In A, the angle demonstrates orientation in the general direction (~30°) of the aggregation center, the source of the wave. In B, the angle (~90°) suggests random direction. (**C**) Measurements of angles for parental Ax2 (WT) and *iplA*⁻ cells. Average angle ± standard deviation is calculated for each cell in four to five successive waves. (**D**) Model in which a short-lived Ca^{2+} gradient (red line) is generated between cells at the onset of each cAMP wave, the latter relayed through the population.

plasma membrane, but at far lower density (Fujimoto et al., 1995; Joseph, 1996; Dellis et al., 2006; Rossier et al., 1991; Fadool and Ache, 1994; Taylor et al., 2009a; Taylor et al., 2009b; Barrera et al., 2007; Bezprozvanny, 2005; Delmas et al., 2002; Tanimura et al., 2000; Tojyo et al., 2008). The possible role of InsP_3Rs in Ca^{2+} chemotaxis had never before been considered or tested.

The role of IplA in Ca^{2+}-facilitated motility and cAMP chemotaxis

By mutational analysis we previously demonstrated that in buffer lacking added Ca^{2+}, the facilitation of motility by K^+ and the requirement of K^+ or Na^+ for chemotactic orientation in a spatial gradient of cAMP (Lusche et al., 2011) are regulated by Nhe1 (Lusche et al., 2011), a putative monovalent cation/hydrogen exchanger in the plasma membrane of *D. discoideum* (Patel and Barber, 2005). The alternative cationic facilitation of these behaviors by Ca^{2+} in the null mutant *nhe1*⁻, however, was completely intact (Lusche et al., 2011), leading us to conclude that Nhe1 mediates monovalent cation effects on behavior, and that one or more other surface molecules mediate alternative Ca^{2+} effects. In the present study we found that IplA plays a role in the Ca^{2+} facilitation of velocity in buffer and in a spatial gradient of cAMP, but it plays no role in the Ca^{2+} or K^+ requirement for chemotactic orientation in a spatial gradient of cAMP. We also found that IplA plays no role in the chemokinetic responsiveness of cells to increasing temporal gradients of cAMP generated in vitro (Varnum et al., 1985; Soll et al., 2002). Our previous (Lusche et al., 2010) and present results, therefore, demonstrate that although all of the K^+ or Na^+ effects on basic behavior and cAMP chemotaxis are mediated by Nhe1, only selective Ca^{2+} effects on basic behavior are mediated by IplA. These results indicate that one or more molecules other than IplA play a role in the Ca^{2+} requirement for chemotactic orientation, a response that involves both the capacity to sense the direction of a cAMP gradient and suppression of lateral pseudopodium formation and turning (Soll et al., 2002).

The localization of IplA

Our analysis of living cells expressing IplA–GFP revealed that fluorescence was primarily cytoplasmic and vesicular. The generation of plasma membrane ghosts revealed very low level staining. Because the preparation of ghosts involved treatment of cells with Triton X-100, a detergent that can disrupt lipids and possibly result in the contamination of plasma membranes with vesicular membranes, we can only tentatively conclude that IplA might be localized in the plasma membrane. But other observations add support to a cell surface role for IplA. Results by Traynor et al. suggested that IplA was involved in extracellular Ca^{2+} uptake and therefore might function as a Ca^{2+} channel at the surface of the cell (Traynor et al., 2000). Uptake, however, could also be mediated through the intracellular regulation of Ca^{2+} stores. Schaloske et al. have presented evidence that the main role of IplA could be in intracellular homeostasis (Schaloske et al., 2005). Shanley et al. subsequently demonstrated that *iplA*⁻ cells underwent electrotaxis, which depends on regulated Ca^{2+} influx, indicating that IplA is not the cell surface Ca^{2+} influx channel for electrotaxis (Shanley et al., 2006). However, the mechanoreception defect in *iplA*⁻ cells lends support to a possible role of IplA at the plasma membrane. Mutant *iplA*⁻ cells lose the orientation response in the direction of fluid flow and cannot attain shear-induced maximum velocity (Fache et al., 2005; Lombardi et al., 2008), suggesting that it functions as a mechanoreceptor at the surface of the cell. However, these results can be just as cogently explained by a role for IplA in a signal transduction pathway downstream of an unidentified mechanoreceptor. Our observation that there is a reduction in Ca^{2+} binding at the surface of *iplA*⁻ cells are consistent with cell surface localization, but could just as well reflect an indirect decrease in another plasma membrane Ca^{2+}-binding protein that depends upon IplA for membrane localization. Therefore, although there is no definitive proof that IplA is a surface receptor, the possibility remains viable.

IplA is necessary for Ca^{2+} chemotaxis

Perhaps the most interesting defect of the *iplA*⁻ mutant is the loss of Ca^{2+} chemotaxis. We generated a variety of Ca^{2+} gradients in

microfluidic chambers with different shapes and different concentration ranges, but *iplA*$^{-}$ chemotaxis was never observed (data not shown). These results suggest that either IplA functions at the cell surface as a receptor for Ca^{2+} chemotaxis, or another, unidentified molecule in the plasma membrane acts as the Ca^{2+} chemotaxis receptor and transduction of the signal produced by an intracellular Ca^{2+} gradient through this unidentified receptor depends on IplA, either at the cell surface or intracellularly.

If IplA proves to be the bona fide surface receptor for Ca^{2+} chemotaxis, it must be coupled to relevant signal transduction pathways in order to elicit directed movement up a spatial gradient of Ca^{2+} (Brown and MacLeod, 2001; Brown et al., 1993; Khan and Conigrave, 2010; Magno et al., 2011; Huang et al., 2002; Huang et al., 2004; Handlogten et al., 2001; Ward, 2004). Given the similarities between cell behavior during chemotaxis in a spatial gradient of Ca^{2+} and behavior in a spatial gradient of cAMP (Scherer et al., 2010), one would expect downstream convergence of the Ca^{2+} and cAMP signal transduction pathways. Coupling of the receptors to the G-protein complex (Wang et al., 2011; Garcia and Parent, 2008; Swaney et al., 2010) might represent an upstream point of convergence. Because IplA is an inositol trisphosphate receptor-like protein (Traynor et al., 2000) and phospholipase C is activated to form InsP_3 when cAMP receptors are stimulated by a global cAMP signal (Europe-Finner and Newell, 1987; Drayer et al., 1994; Kortholt et al., 2007; King et al., 2009), IplA might function downstream of a similar Ca^{2+}-induced system. Hence, convergence of the cAMP and Ca^{2+} pathways might occur downstream of that interaction. The possible convergence of the signal transduction pathways of the chemotactic response to spatial gradients of cAMP and Ca^{2+}, and, hence, the sharing of downstream components of a common signal transduction pathway, could explain, in part, why the two chemotactic systems are acquired at roughly the same time in the developmental program of *D. discoideum* (Scherer et al., 2010).

IplA is required for chemotaxis in a natural wave

In vitro analyses performed here and previously (Traynor et al., 2000) revealed that chemotaxis up a spatial gradient of cAMP is intact in the *iplA*$^{-}$ mutant. Additional analyses performed here revealed that the chemokinetic response to the increasing phase of a temporal camp wave generated in vitro was also intact. We previously argued that these in vitro assays tested the full complement of responses to the spatial and temporal dynamics of a naturally relayed cAMP wave (Soll et al., 2002). We therefore fully expected *iplA*$^{-}$ cells to function normally during natural aggregation, based on the assumption that the cAMP wave represented the exclusive natural chemotactic signal. However, the response of minority *iplA*$^{-}$ cells seeded in a natural aggregation territory of majority parental wild-type Ax2 cells was highly aberrant. Although *iplA*$^{-}$ cells exhibited increases in velocity (i.e. velocity surges) that correlated with the velocity surges of neighboring majority Ax2 cells in the front of consecutive natural cAMP waves relayed by the majority wild-type cell populations, they did not reorient towards the aggregation center at the onset of each new wave, as was the case for neighboring parental wild-type cells (Wessels et al., 1992; Soll et al., 2002).

A new model for chemotaxis

Because Bonner and colleagues (Konijn et al., 1969) first demonstrated that the chemotactic agent in natural *D. discoideum* aggregation territories was cAMP, and Tomchik and Devreotes then provided fixed images of cAMP waves (Tomchik and Devreotes, 1981), it has been assumed that cAMP is the sole chemoattractant during natural aggregation. Upon discovering that *D. discoideum* amoebae also underwent chemotaxis in Ca^{2+} gradients, and that cAMP and Ca^{2+} chemotaxis were acquired at similar times in the developmental program, we suggested that Ca^{2+} chemotaxis also plays a role in natural aggregation, although at the time of that suggestion, we had no evidence that it indeed played such a role (Scherer et al., 2010). Because global stimulation by cAMP causes a rapid uptake and then release of Ca^{2+} by aggregation-competent cells (Bumann et al., 1984; Bumann et al., 1986; Wick et al., 1978), we considered the possibility that this represents a process that takes place at the onset of each natural wave, leading to the establishment of a transient Ca^{2+} gradient between cells (Fig. 8D). In turn, a rapid chemotactic response of cells at the onset of a natural wave to such a transient Ca^{2+} gradient might mediate or augment reorientation towards the aggregation center (Scherer et al., 2010). Because Ca^{2+} has so high a diffusion rate, the possibility of a relayed Ca^{2+} wave cannot be entertained (Scherer et al., 2010). This hypothesis (Fig. 8D) would explain our observation that *iplA*$^{-}$ cells surge in response to the increasing temporal gradient in the front of each natural cAMP wave, but have trouble reorienting in the direction of the aggregation center. This hypothesis warrants further investigation. If it proves correct, it would alter our view of natural *D. discoideum* chemotaxis, and provide an expanded contextual framework for interpreting motility and chemotaxis mutants.

Materials and Methods

Strain maintenance, growth and development

The parental *Dictyostelium discoideum* Ax2 strain and the *iplA*$^{-}$ mutant, HM1038 (Traynor et al., 2000), were obtained from the *Dictyostelium* stock center (http://dictybase.org/StockCenter/StockCenter.html) and subcloned. Cells were reconstituted from frozen stocks every 2 weeks (Varnum et al., 1986), and grown in HL-5 medium (http://dictybase.org/techniques/index.html) supplemented with 10 μg/ml of blasticidin S (Sigma-Aldrich). The ip*lA*$^{-}$/*iplA*$^{+}$-GFP derivative (see below) was grown in both 10 μg/ml blasticidin S and 20 μg/ml of G418 (Sigma-Aldrich). Aggregation-competent cells were obtained according to methods previously described (Soll, 1979).

Generating *iplA*$^{-}$/*iplA*$^{+}$-GFP cells

Total RNA was extracted using Trizol (Invitrogen, Carlsbad, CA) and RT-PCR performed using the Long Range RT-PCR kit (Qiagen, Hilden, Germany) according to manufacturer's instructions. The 9534 bp *iplA* cDNA was amplified using the Roche Long Template PCR Kit (Roche Applied Sciences, Indianapolis, IN) according to manufacturer's instructions. The primers used were Kpn forward (5′-AAATCGGGGTACCATGGAAGAGAAAAATGTTAATTTGAAA-3′) and *iplA* KPN reverse (5′-CGGGGTACCTTTTTGTTGTTGTTTTAAATCACTAAC-3′). Underlines indicate restriction sites. The ligated plasmid was transformed into DH5α max efficiency *Escherichia coli*. The amplified plasmid was then isolated using the Rapid Plasmid Purification Kit (Marligen, Ijamsville, MD). The Gateway recombination cloning system (Invitrogen) was used for tagging the N-terminus of the *iplA* cDNA with GFP. PCR was performed with the pTOPO-XL-iplA plasmid as template, using the primers 5′-CACCATGGAAGAGAAAAATGTTAATT-TGAAAACC-3′ (cloning site underlined) and 5′-CGTTCGTTGCCGGCTT-ATTTTTGTTGTTGTTTTAAATCACTAACTTGTTGTC-3′ (restriction site underlined). The resulting cDNA fragment was purified using the Qiagen PCR Purification Kit (Qiagen) and digested with *Nae*I (NEB, Ipswich, MA) to generate a blunt end. The digested fragments were dephosphorylated using calf intestine phosphatase (NEB) and the fragments purified in a TAE (40 mM Tris-HCl, 20 mM acetic acid, 1 mM EDTA, pH 8.0) gel. The resulting *iplA* cDNA was ligated into the plasmid pENTR-D (Invitrogen) at a 1:2 ratio and the ligation construct transformed into TOP10-competent cells. To derive the N-terminal GFP–*iplA* fusion, the *D. discoideum* extrachromosomal plasmid pDM351 (Veltman et al., 2009), obtained from the Dictybase stock center http://dictybase.org/StockCenter/StockCenter.html), was used for recombination with the plasmid pENTR-D-iplA. pDM351 carries pENTR-D-specific recombination sites, an actin15-driven

N-terminal GFP expression cassette and a neomycin resistance cassette for positive selection. To perform recombination, equal amounts of pENTR-D-iplA and pDM351 were incubated overnight in the presence of Gateway-LR Clonase (Invitrogen). The reaction was terminated by addition of protein kinase K according to the manufacturer's (Invitrogen) instructions. Cells were transformed into TOP10-competent cells and positive clones were identified by colony PCR. The N-terminal fusion of GFP to *iplA*$^+$ in pDM351-iplA was confirmed by sequencing. The plasmid pDM351-iplA$^+$ was transformed into *iplA*$^-$ cells as described previously (Lusche et al., 2011; Wessels et al., 2007). Positive cells (*iplA*$^-$/*iplA*$^+$-GFP) from growth plates were sorted by fluorescent-activated cell sorting (FACS).

$^{45}Ca^{2+}$ binding

Aggregation-competent cells were washed in Tricine buffer (TB) and incubated for 1 hour in TB containing 10 mM Ca^{2+} (Lusche et al., 2009; Scherer et al., 2010; Lusche et al., 2011). Cells were then washed in TB + 10 mM Ca^{2+} and 6×10^6 cells incubated in 5 mM NaN_3 in TB. After 30 minutes, 1 µCi $^{45}CaCl_2$ (American Radiolabeled Chemicals, St. Louis, MO) was added, the cells were incubated for 5 minutes on ice and pelleted, and the pellet resuspended in 100 µl TB. The suspension was then transferred immediately to 10 ml Ultima Gold liquid scintillation cocktail (Perkin Elmer, Waltham, MA) and dissolved overnight. Parental control and *iplA*$^-$ cells were treated in parallel and measured in duplicate. Samples were counted using a liquid scintillation counter (Packard, Perkin Elmer). Background counts were assessed by counting an aliquot of cells that had been incubated in the absence of $^{45}Ca^{2+}$. The protein content of the samples was measured using the NanoDrop (Thermo Scientific, Wilmington, DE). The percentage reduction in binding by mutant cells was assessed by comparing binding to wild-type cells (100%) in each experiment.

GFP localization by direct detection

For direct detection of GFP fluorescence, *iplA*$^-$/*iplA*$^+$-GFP cells were grown in low fluorescence axenic medium (http://dictybase.org/techniques/index.html). Cells were then developed to aggregation stage, washed as previously described (Lusche et al., 2009) and dispersed on a coverslip in 10 mM Ca^{2+}. Images of live cells were gathered with a Bio-Rad Radiance 2100MP laser scanning system (Bio-Rad Microscience Ltd., Hemel Hempstead, UK) attached to a TE2000E microscope (Nikon USA Ltd., Melville, NY) using a Nikon 60× PLAN APO 1.2 immersion objective. GFP was excited at 488 nm with an argon laser at 10% power. Images of live cells were collected in a single optical plane 1.4 µm above the substratum by accumulated scans over an 8-second period. Simultaneously, a different interference contrast image was also collected for each accumulated fluorescence image. All images were processed using Adobe Photoshop™ software (San Jose, CA). To test for localization at the plasma membrane, Triton-X-100-extracted plasma membrane ghosts were generated by the method of Condeelis (Condeelis, 1979). Briefly, *iplA*$^-$/*iplA*$^+$-GFP or *iplA*$^-$ cells were developed on nitrocellulose filters. Aggregation-competent cells were washed in 20 mM Na^+/K^+ phosphate buffer. Cells were incubated for 2 minutes in 50 µg/ml of concavalin A (Sigma-Aldrich) and resuspended in ice-cold Tris-EDTA buffer pH 7.6. Cells were immediately lysed in an ice-cold solution containing 1 mM EDTA, 5 mM Tris and 0.2% Triton X-100, pH 7.6. Unlysed cells were removed by centrifugation at 480 ***g***. The supernatant was then centrifuged at 2000 ***g*** and the denser pellet removed. The pellet of plasma membrane ghosts was washed in Tris-EDTA buffer. Ghosts were resuspended and visualized using a Bio-Rad Radiance 2100MP laser scanning system (Bio-Rad Microscience Ltd.) attached to a TE2000E microscope (Nikon USA Ltd., Melville, NY) using Nikon Plan Fluor 20× objective. GFP was excited with an argon laser line at 488 nm. All images were processed using Adobe Photoshop™ software.

DIAS analysis of behavior

Cell images were digitally acquired using iStopMotion (Boinx Software, www.boinx.com) software and converted to QuickTime™ (www.apple.com/quicktime) format for analysis with two-dimensional (2D) DIAS [Dynamic Image Analysis System (Soll and Voss, 1998)] software as previously described (Soll, 1995; Wessels et al., 2009). Instantaneous velocity, percentage cells ≥9 µm/minute, directional persistence, chemotactic index and percentage positive chemotaxis were computed from centroid positions (Soll, 1995; Soll and Voss, 1998; Wessels et al., 2009; Scherer et al., 2010). Instantaneous velocity was computed at 4-second intervals between each consecutive pair over a 2-minute period by centroids methods, previously described in detail (Maron, 1982; Soll, 1995; Soll and Voss, 1998). The mean instantaneous velocity was computed from the averages of over 20 cells, each individually analyzed. The parameter percentage cells ≥9 µm/minute was computed as the proportion of cells in a population moving with average instantaneous velocity greater than or equal to 9 µm/minute. The percentage was computed for over 20 cells, each individually analyzed. The positive flow parameter was computed by overlapping perimeter outlines of two consecutive cell images, calculating the area in the second of the two images that did not overlap the first, and expressing that non-overlapping area as a percentage of the area of the first image. This was performed at 4-second intervals over a 10-minute period for each cell, and the mean (± standard deviation) computed from the data of over 20 cells. Directional persistence was computed as the net distance between the first and last centroid of a centroid track divided by the summed distances between consecutive centroid positions of the track. The centroids were computed for each of over 20 cells at 4-second intervals over a 10-minute period. The chemotactic index (CI) was computed as the net distance traveled in the direction of the cAMP source divided by the total distance traveled. The mean CI (± standard deviation) was then computed from the data of over 20 cells. A CI of –1.00 indicated direct movement down the gradient, +1.00 indicated direct movement up the gradient, 0.00 indicated random movement, and +0.01 to +0.99 indicated increasing levels of positive chemotaxis. The rightward directionality (RD) parameter is defined in the results section. The percentage positive chemotaxis parameter was measured as the proportion of cells in a population with a chemotactic index greater than 0.00.

Mixing experiments for natural aggregation

To analyze the behavior of *iplA*$^-$ cells in wild-type aggregation territories, mutant cells were labeled with the vital dye DiI (Invitrogen), mixed with a majority of unlabeled Ax2 cells, and motion was analyzed during aggregation according to methods described in detail elsewhere (Wessels et al., 2004; Heid et al., 2004). Briefly, *iplA*$^-$ cells were labeled by incubation in HL-5 containing 0.05 mM DiI (Invitrogen) for 24 hours in the dark. Control Ax2 cells were treated similarly, but in the absence of DiI. HL-5 was then removed from labeled *iplA*$^-$ cells and unlabeled vegetative Ax2 cells by washing in buffered salt solution (20 mM KCl, 2.5 mM $MgCl_2$, 20 mM KH_2PO_4 and 5 mM Na_2HPO_4, pH 6.4) (Sussman, 1987) in which K^+ was the facilitating cation (Lusche et al., 2011). The Ax2 and labeled *iplA*$^-$ cell populations were then mixed at a 9:1 ratio to yield 5×10^6 cells per 2 ml. This suspension was inoculated into a 35 mm Petri dish and the dish placed on the stage of a Nikon Eclipse TE-2000 microscope connected to a Bio-Rad Radiance 2100MP laser scanning confocal microscope (Bio-Rad Microscience Ltd.). After 6 hours, image acquisition was begun using a green HeNe laser at 543 nm, a 10× objective and a 2.2 digital zoom. A signal-enhancing lens and an emission filter HQ 590/70 were included in the light path. Transmitted light images were continuously collected through a transmitted light detector at 543 nm. Cells were exposed to laser light every 30 seconds with a laser intensity of 19.7% for DiI excitation and 2.8% for the transmitted light. Transmitted and fluorescence images were collected through the photomultiplier tube with LaserSharp 2000 software (release 5.2) and converted to a QuickTime™ format. Labeled *iplA*$^-$ cells and unlabeled Ax2 cells were outlined from the QuickTime™ movie and motion analyzed using 2D-DIAS as described above.

Acknowledgements

We are grateful to Kristin Weigel and Vanja Stojkovic for help with the Ca^{2+}-binding studies.

Funding

This work was supported by the Developmental Studies Hybridoma Bank, a National Resource originally established by the National Institutes of Health. Deposited in PMC for release after 12 months.

Supplementary material available online at
http://jcs.biologists.org/lookup/suppl/doi:10.1242/jcs.098301/-/DC1

References

Barrera, N. P., Morales, B. and Villalon, M. (2007). ATP and adenosine trigger the interaction of plasma membrane IP3 receptors with protein kinase A in oviductal ciliated cells. *Biochem. Biophys. Res. Commun.* **364**, 815-821.

Bezprozvanny, I. (2005). The inositol 1,4,5-trisphosphate receptors. *Cell Calcium* **38**, 261-272.

Blondel, O., Takeda, J., Janssen, H., Seino, S. and Bell, G. I. (1993). Sequence and functional characterization of a third inositol trisphosphate receptor subtype, IP3R-3, expressed in pancreatic islets, kidney, gastrointestinal tract, and other tissues. *J. Biol. Chem.* **268**, 11356-11363.

Boudot, C., Saidak, Z., Boulanouar, A. K., Petit, L., Gouilleux, F., Massy, Z., Brazier, M., Mentaverri, R. and Kamel, S. (2010). Implication of the calcium sensing receptor and the Phosphoinositide 3-kinase/Akt pathway in the extracellular calcium-mediated migration of RAW 264.7 osteoclast precursor cells. *Bone* **46**, 1416-1423.

Brown, E. M. and MacLeod, R. J. (2001). Extracellular calcium sensing and extracellular calcium signaling. *Physiol. Rev.* **81**, 239-297.

Brown, E. M., Gamba, G., Riccardi, D., Lombardi, M., Butters, R., Kifor, O., Sun, A., Hediger, M. A., Lytton, J. and Hebert, S. C. (1993). Cloning and characterization of an extracellular Ca(2+)-sensing receptor from bovine parathyroid. *Nature* **366**, 575-580.

Bumann, J., Wurster, B. and Malchow, D. (1984). Attractant-induced changes and oscillations of the extracellular Ca^{++} concentration in suspensions of differentiating *Dictyostelium* cells. *J. Cell Biol.* **98**, 173-178.

Bumann, J., Malchow, D. and Wurster, B. (1986). Oscillations of Ca^{++} concentration during the cell differentiation of *Dictyostelium discoideum*. *Differentiation* **31**, 85-91.
Condeelis, J. (1979). Isolation of concanavalin A caps during various stages of formation and their association with actin and myosin. *J. Cell Biol.* **80**, 751-758.
da Fonseca, P. C., Morris, S. A., Nerou, E. P., Taylor, C. W. and Morris, E. P. (2003). Domain organization of the type 1 inositol 1,4,5-trisphosphate receptor as revealed by single-particle analysis. *Proc. Natl. Acad. Sci. USA* **100**, 3936-3941.
Dellis, O., Dedos, S. G., Tovey, S. C., Taufiq-Ur-Rahman, Dubel, S. J. and Taylor, C. W. (2006). Ca^{2+} entry through plasma membrane IP3 receptors. *Science* **313**, 229-233.
Delmas, P., Wanaverbecq, N., Abogadie, F. C., Mistry, M. and Brown, D. A. (2002). Signaling microdomains define the specificity of receptor-mediated InsP(3) pathways in neurons. *Neuron* **34**, 209-220.
Devreotes, P. N. and Steck, T. L. (1979). Cyclic 3′,5′ AMP relay in *Dictyostelium discoideum*. II. Requirements for the initiation and termination of the response. *J. Cell Biol.* **80**, 300-309.
Devreotes, P. N., Potel, M. J. and MacKay, S. A. (1983). Quantitative analysis of cyclic AMP waves mediating aggregation in *Dictyostelium discoideum*. *Dev. Biol.* **96**, 405-415.
Drayer, A. L., Van der Kaay, J., Mayr, G. W. and Van Haastert, P. J. (1994). Role of phospholipase C in *Dictyostelium*: formation of inositol 1,4,5-trisphosphate and normal development in cells lacking phospholipase C activity. *EMBO J.* **13**, 1601-1609.
Europe-Finner, G. N. and Newell, P. C. (1987). Cyclic AMP stimulates accumulation of inositol trisphosphate in *Dictyostelium*. *J. Cell Sci.* **87**, 221-229.
Fache, S., Dalous, J., Engelund, M., Hansen, C., Chamaraux, F., Fourcade, B., Satre, M., Devreotes, P. and Bruckert, F. (2005). Calcium mobilization stimulates *Dictyostelium discoideum* shear-flow-induced cell motility. *J. Cell Sci.* **118**, 3445-3457.
Fadool, D. A. and Ache, B. W. (1994). Inositol 1,3,4,5-tetrakisphosphate-gated channels interact with inositol 1,4,5-trisphosphate-gated channels in olfactory receptor neurons. *Proc. Natl. Acad. Sci. USA* **91**, 9471-9475.
Ferris, C. D., Huganir, R. L., Supattapone, S. and Snyder, S. H. (1989). Purified inositol 1,4,5-trisphosphate receptor mediates calcium flux in reconstituted lipid vesicles. *Nature* **342**, 87-89.
Foskett, J. K. (2010). Inositol trisphosphate receptor Ca^{2+} release channels in neurological diseases. *Pflügers Arch.* **460**, 481-494.
Foskett, J. K., White, C., Cheung, K. H. and Mak, D. O. (2007). Inositol trisphosphate receptor Ca^{2+} release channels. *Physiol. Rev.* **87**, 593-658.
Fujimoto, T., Miyawaki, A. and Mikoshiba, K. (1995). Inositol 1,4,5-trisphosphate receptor-like protein in plasmalemmal caveolae is linked to actin filaments. *J. Cell Sci.* **108**, 7-15.
Furuichi, T., Yoshikawa, S., Miyawaki, A., Wada, K., Maeda, N. and Mikoshiba, K. (1989). Primary structure and functional expression of the inositol 1,4,5-trisphosphate-binding protein P400. *Nature* **342**, 32-38.
Garcia, G. L. and Parent, C. A. (2008). Signal relay during chemotaxis. *J. Microsc.* **231**, 529-534.
Garrett, J. E., Capuano, I. V., Hammerland, L. G., Hung, B. C., Brown, E. M., Hebert, S. C., Nemeth, E. F. and Fuller, F. (1995). Molecular cloning and functional expression of human parathyroid calcium receptor cDNAs. *J. Biol. Chem.* **270**, 12919-12925.
Gerisch, G., Normann, I. and Beug, H. (1966). [Rhythm of cell orientation and velocity of movement in the chemotactic reaction system of *Dictyostelium discoideum*]. *Naturwissenschaften* **53**, 618.
Groner, M. and Malchow, D. (1996). Calmodulin-antagonists inhibit vesicular Ca^{2+} uptake in *Dictyostelium*. *Cell Calcium* **19**, 105-111.
Handlogten, M. E., Huang, C., Shiraishi, N., Awata, H. and Miller, R. T. (2001). The Ca^{2+}-sensing receptor activates cytosolic phospholipase A2 via a Gqalpha-dependent ERK-independent pathway. *J. Biol. Chem.* **276**, 13941-13948.
Heid, P. J., Wessels, D., Daniels, K. J., Gibson, D. P., Zhang, H., Voss, E. and Soll, D. R. (2004). The role of myosin heavy chain phosphorylation in *Dictyostelium* motility, chemotaxis and F-actin localization. *J. Cell Sci.* **117**, 4819-4835.
Huang, C., Handlogten, M. E. and Miller, R. T. (2002). Parallel activation of phosphatidylinositol 4-kinase and phospholipase C by the extracellular calcium-sensing receptor. *J. Biol. Chem.* **277**, 20293-20300.
Huang, C., Hujer, K. M., Wu, Z. and Miller, R. T. (2004). The Ca^{2+}-sensing receptor couples to Galpha12/13 to activate phospholipase D in Madin-Darby canine kidney cells. *Am. J. Physiol. Cell Physiol.* **286**, C22-C30.
Joseph, S. K. (1996). The inositol triphosphate receptor family. *Cell. Signal.* **8**, 1-7.
Khan, M. A. and Conigrave, A. D. (2010). Mechanisms of multimodal sensing by extracellular Ca(2+)-sensing receptors: a domain-based survey of requirements for binding and signalling. *Br. J. Pharmacol.* **159**, 1039-1050.
King, J. S., Teo, R., Ryves, J., Reddy, J. V., Peters, O., Orabi, B., Hoeller, O., Williams, R. S. and Harwood, A. J. (2009). The mood stabiliser lithium suppresses PIP3 signalling in *Dictyostelium* and human cells. *Dis. Model. Mech.* **2**, 306-312.
Konijn, T. M., Van De Meene, J. G., Bonner, J. T. and Barkley, D. S. (1967). The acrasin activity of adenosine-3′,5′-cyclic phosphate. *Proc. Natl. Acad. Sci. USA* **58**, 1152-1154.
Konijn, T. M., van de Meene, J. G., Chang, Y. Y., Barkley, D. S. and Bonner, J. T. (1969). Identification of adenosine-3′,5′-monophosphate as the bacterial attractant for myxamoebae of *Dictyostelium discoideum*. *J. Bacteriol.* **99**, 510-512.
Kortholt, A., King, J. S., Keizer-Gunnink, I., Harwood, A. J. and Van Haastert, P. J. (2007). Phospholipase C regulation of phosphatidylinositol 3,4,5-trisphosphate-mediated chemotaxis. *Mol. Biol. Cell* **18**, 4772-4779.
Lombardi, M. L., Knecht, D. A. and Lee, J. (2008). Mechano-chemical signaling maintains the rapid movement of *Dictyostelium* cells. *Exp. Cell Res.* **314**, 1850-1859.
Lusche, D. F., Wessels, D. and Soll, D. R. (2009). The effects of extracellular calcium on motility, pseudopod and uropod formation, chemotaxis, and the cortical localization of myosin II in *Dictyostelium discoideum*. *Cell Motil. Cytoskeleton* **66**, 567-587.
Lusche, D. F., Wessels, D., Ryerson, D. E. and Soll, D. R. (2011). Nhe1 is essential for potassium but not calcium facilitation of cell motility and the monovalent cation requirement for chemotactic orientation in *Dictyostelium discoideum*. *Eukaryot. Cell* **10**, 320-331.
Maeda, N., Kawasaki, T., Nakade, S., Yokota, N., Taguchi, T., Kasai, M. and Mikoshiba, K. (1991). Structural and functional characterization of inositol 1,4,5-trisphosphate receptor channel from mouse cerebellum. *J. Biol. Chem.* **266**, 1109-1116.
Magno, A. L., Ward, B. K. and Ratajczak, T. (2011). The calcium-sensing receptor: a molecular perspective. *Endocr. Rev.* **32**, 3-30.
Maranto, A. R. (1994). Primary structure, ligand binding, and localization of the human type 3 inositol 1,4,5-trisphosphate receptor expressed in intestinal epithelium. *J. Biol. Chem.* **269**, 1222-1230.
Maron, M. (1982). *Numerical Analysis: A Practical Approach*. New York: Macmillan.
Mignery, G. A. and Sudhof, T. C. (1990). The ligand binding site and transduction mechanism in the inositol-1,4,5-triphosphate receptor. *EMBO J.* **9**, 3893-3898.
Milne, J. L. and Coukell, M. B. (1991). A Ca^{2+} transport system associated with the plasma membrane of *Dictyostelium discoideum* is activated by different chemoattractant receptors. *J. Cell Biol.* **112**, 103-110.
Milne, J. L. and Devreotes, P. N. (1993). The surface cyclic AMP receptors, cAR1, cAR2, and cAR3, promote Ca^{2+} influx in *Dictyostelium discoideum* by a G alpha 2-independent mechanism. *Mol. Biol. Cell* **4**, 283-292.
Patel, H. and Barber, D. L. (2005). A developmentally regulated Na-H exchanger in *Dictyostelium discoideum* is necessary for cell polarity during chemotaxis. *J. Cell Biol.* **169**, 321-329.
Patterson, R. L., Boehning, D. and Snyder, S. H. (2004). Inositol 1,4,5-trisphosphate receptors as signal integrators. *Annu. Rev. Biochem.* **73**, 437-465.
Ramos-Franco, J., Galvan, D., Mignery, G. A. and Fill, M. (1999). Location of the permeation pathway in the recombinant type 1 inositol 1,4,5-trisphosphate receptor. *J. Gen. Physiol.* **114**, 243-250.
Ross, C. A., Danoff, S. K., Schell, M. J., Snyder, S. H. and Ullrich, A. (1992). Three additional inositol 1,4,5-trisphosphate receptors: molecular cloning and differential localization in brain and peripheral tissues. *Proc. Natl. Acad. Sci. USA* **89**, 4265-4269.
Rossier, M. F., Bird, G. S. and Putney, J. W., Jr (1991). Subcellular distribution of the calcium-storing inositol 1,4,5-trisphosphate-sensitive organelle in rat liver. Possible linkage to the plasma membrane through the actin microfilaments. *Biochem. J.* **274**, 643-650.
Schaloske, R. H., Lusche, D. F., Bezares-Roder, K., Happle, K., Malchow, D. and Schlatterer, C. (2005). Ca^{2+} regulation in the absence of the *iplA* gene product in *Dictyostelium discoideum*. *BMC Cell Biol.* **6**, 13.
Scherer, A., Kuhl, S., Wessels, D., Lusche, D. F., Raisley, B. and Soll, D. R. (2010). Ca^{2+} chemotaxis in *Dictyostelium discoideum*. *J. Cell Sci.* **123**, 3756-3767.
Shanley, L. J., Walczysko, P., Bain, M., MacEwan, D. J. and Zhao, M. (2006). Influx of extracellular Ca^{2+} is necessary for electrotaxis in *Dictyostelium*. *J. Cell Sci.* **119**, 4741-4748.
Soll, D. and Voss, E. (1998). Two and three dimensional computer systems for analyzing how cells crawl. In *Motion Analysis Of Living Cells* (ed. D. Soll and D. Wessels), pp. 5-52. New York: Wiley-Liss.
Soll, D., Wessels, D., Lusche, D. F., Kuhl, S., Scherer, A. and Grimm, S. (2011). Role of extracellular cations in cell motility, polarity, and chemotaxis. *Res. Rep. Biol.* **2**, 69-88.
Soll, D. R. (1979). Timers in developing systems. *Science* **203**, 841-849.
Soll, D. R. (1995). The use of computers in understanding how animal cells crawl. *Int. Rev. Cytol.* **163**, 43-104.
Soll, D. R., Wessels, D., Heid, P. J. and Zhang, H. (2002). A contextual framework for characterizing motility and chemotaxis mutants in *Dictyostelium discoideum*. *J. Muscle Res. Cell Motil.* **23**, 659-672.
Stepanovic, V., Wessels, D., Daniels, K., Loomis, W. F. and Soll, D. R. (2005). Intracellular role of adenylyl cyclase in regulation of lateral pseudopod formation during *Dictyostelium* chemotaxis. *Eukaryot. Cell* **4**, 775-786.
Sudhof, T. C., Newton, C. L., Archer, B. T., 3rd, Ushkaryov, Y. A. and Mignery, G. A. (1991). Structure of a novel InsP3 receptor. *EMBO J.* **10**, 3199-3206.
Sussman, M. (1987). Cultivation and synchronous morphogenesis of *Dictyostelium* under controlled experimental conditions. *Methods Cell Biol.* **28**, 9-29.
Swaney, K. F., Huang, C. H. and Devreotes, P. N. (2010). Eukaryotic chemotaxis: a network of signaling pathways controls motility, directional sensing, and polarity. *Annu. Rev. Biophys.* **39**, 265-289.
Tanimura, A., Tojyo, Y. and Turner, R. J. (2000). Evidence that type I, II, and III inositol 1,4,5-trisphosphate receptors can occur as integral plasma membrane proteins. *J. Biol. Chem.* **275**, 27488-27493.
Taylor, C. W. and Laude, A. J. (2002). IP3 receptors and their regulation by calmodulin and cytosolic Ca^{2+}. *Cell Calcium* **32**, 321-334.

Taylor, C. W., Taufiq-Ur-Rahman and Pantazaka, E. (2009a). Targeting and clustering of IP3 receptors: key determinants of spatially organized Ca^{2+} signals. *Chaos* **19**, 037102.

Taylor, C. W., Rahman, T., Tovey, S. C., Dedos, S. G., Taylor, E. J. and Velamakanni, S. (2009b). IP3 receptors: some lessons from DT40 cells. *Immunol. Rev.* **231**, 23-44.

Tojyo, Y., Morita, T., Nezu, A. and Tanimura, A. (2008). The clustering of inositol 1,4,5-trisphosphate (IP(3)) receptors is triggered by IP(3) binding and facilitated by depletion of the Ca(2+) store. *J. Pharmacol. Sci.* **107**, 138-150.

Tomchik, K. J. and Devreotes, P. N. (1981). Adenosine 3′,5′-monophosphate waves in *Dictyostelium discoideum*: a demonstration by isotope dilution-fluorography. *Science* **212**, 443-446.

Traynor, D., Milne, J. L., Insall, R. H. and Kay, R. R. (2000). Ca(2+) signalling is not required for chemotaxis in *Dictyostelium*. *EMBO J.* **19**, 4846-4854.

Vannier, B., Zhu, X., Brown, D. and Birnbaumer, L. (1998). The membrane topology of human transient receptor potential 3 as inferred from glycosylation-scanning mutagenesis and epitope immunocytochemistry. *J. Biol. Chem.* **273**, 8675-8679.

Varnum, B. and Soll, D. R. (1984). Effects of cAMP on single cell motility in *Dictyostelium*. *J. Cell Biol.* **99**, 1151-1155.

Varnum, B., Edwards, K. B. and Soll, D. R. (1985). *Dictyostelium* amebae alter motility differently in response to increasing versus decreasing temporal gradients of cAMP. *J. Cell Biol.* **101**, 1-5.

Varnum, B., Edwards, K. B. and Soll, D. R. (1986). The developmental regulation of single-cell motility in *Dictyostelium discoideum. Dev. Biol.* **113**, 218-227.

Varnum-Finney, B., Edwards, K. B., Voss, E. and Soll, D. R. (1987). Amebae of *Dictyostelium discoideum* respond to an increasing temporal gradient of the chemoattractant cAMP with a reduced frequency of turning: evidence for a temporal mechanism in ameboid chemotaxis. *Cell Motil. Cytoskeleton* **8**, 7-17.

Varnum-Finney, B., Schroeder, N. A. and Soll, D. R. (1988). Adaptation in the motility response to cAMP in *Dictyostelium discoideum*. *Cell Motil. Cytoskeleton* **9**, 9-16.

Veltman, D. M., Akar, G., Bosgraaf, L. and Van Haastert, P. J. (2009). A new set of small, extrachromosomal expression vectors for *Dictyostelium discoideum*. *Plasmid* **61**, 110-118.

Wang, Y., Chen, C. L. and Iijima, M. (2011). Signaling mechanisms for chemotaxis. *Dev. Growth Differ.* **53**, 495-502.

Ward, D. T. (2004). Calcium receptor-mediated intracellular signalling. *Cell Calcium* **35**, 217-228.

Wessels, D. and Soll, D. R. (1990). Myosin II heavy chain null mutant of *Dictyostelium* exhibits defective intracellular particle movement. *J. Cell Biol.* **111**, 1137-1148.

Wessels, D., Murray, J. and Soll, D. R. (1992). Behavior of *Dictyostelium* amoebae is regulated primarily by the temporal dynamic of the natural cAMP wave. *Cell Motil. Cytoskeleton* **23**, 145-156.

Wessels, D., Reynolds, J., Johnson, O., Voss, E., Burns, R., Daniels, K., Garrard, E., O'Halloran, T. J. and Soll, D. R. (2000a). Clathrin plays a novel role in the regulation of cell polarity, pseudopod formation, uropod stability and motility in *Dictyostelium*. *J. Cell Sci.* **113**, 21-36.

Wessels, D. J., Zhang, H., Reynolds, J., Daniels, K., Heid, P., Lu, S., Kuspa, A., Shaulsky, G., Loomis, W. F. and Soll, D. R. (2000b). The internal phosphodiesterase RegA is essential for the suppression of lateral pseudopods during *Dictyostelium* chemotaxis. *Mol. Biol. Cell* **11**, 2803-2820.

Wessels, D., Brincks, R., Kuhl, S., Stepanovic, V., Daniels, K. J., Weeks, G., Lim, C. J., Spiegelman, G., Fuller, D., Iranfar, N. et al. (2004). RasC plays a role in transduction of temporal gradient information in the cyclic-AMP wave of *Dictyostelium discoideum. Eukaryot. Cell* **3**, 646-662.

Wessels, D., Lusche, D. F., Kuhl, S., Heid, P. and Soll, D. R. (2007). PTEN plays a role in the suppression of lateral pseudopod formation during *Dictyostelium* motility and chemotaxis. *J. Cell Sci.* **120**, 2517-2531.

Wessels, D. J., Kuhl, S. and Soll, D. R. (2009). Light microscopy to image and quantify cell movement. *Methods Mol. Biol.* **571**, 455-471.

Wick, U., Malchow, D. and Gerisch, G. (1978). Cyclic-AMP stimulated calcium influx into aggregating cells of *Dictyostelium discoideum*. *Cell Biol. Int. Rep.* **2**, 71-79.

Yule, D. I., Betzenhauser, M. J. and Joseph, S. K. (2010). Linking structure to function: Recent lessons from inositol 1,4,5-trisphosphate receptor mutagenesis. *Cell Calcium* **47**, 469-479.

Zigmond, S. H. (1977). Ability of polymorphonuclear leukocytes to orient in gradients of chemotactic factors. *J. Cell Biol.* **75**, 606-616.

Journal of Cell Science